# MAGNETOSTATIC WAVE PROPAGATION

# IN A YIG CRYSTAL AT 960 MHz

MAGNETOSTATIC WAVE PROPAGATION

IN A YIG CRYSTAL AT 950 MHz

By

CHANDRA MOHAN KUDSIA, B.Sc.(Hons), B.E.

A Thesis

Submitted to the Faculty of Graduate Studies

in Partial Fulfilment of the Requirements

for the Degree

Master of Engineering

McMaster University

May 1966

MASTER OF ENGINEERING (1966)
(Electrical)

McMASTER UNIVERSITY
Hamilton, Ontario.

TITLE: Magnetostatic Wave Propagation in a YIG Crystal at 950 MHz.

AUTHOR: Chandra Mohan Kudsia, B.Sc.(Hons), B.E.

SUPERVISORS: Professor M. W. Gunn

Professor J. K. Campbell

NUMBER OF PAGES: vi, 79

SCOPE AND CONTENTS:

Previously reported work on Microwave Ultrasonics is reviewed briefly. Various aspects of the generation, transmission and delay characteristics of elastic, magnetoelastic and spin waves are discussed with due emphasis on the coupling mechanisms.

Magnetostatic waves in the frequency range 890 Mc/s to 990 Mc/s are studied in an axially magnetised, unsaturated single crystal of Yttrium Iron Garnet, cylindrical in shape and oriented along the (100) axis. The design of a strip-line mounting assembly, to couple the energy in and out of the YIG rod, has been outlined. A non-uniform internal magnetic field is proposed and analysed for the unsaturated sample to explain the experimental results.

# ABSTRACT

An investigation has been made of the propagation characteristics of magnetostatic waves with frequencies in the range 890 - 990 MHz in a crystal of Yttrium Iron Garnet. The sample was mounted in a two port strip line assembly and magnetised axially along the (100) direction. The experiments were performed at room temperature.

Magnetostatic waves were observed in external magnetic fields in the neighbourhood of 500 Oersteds, and to explain the experimental results a non-uniform distribution of magnetisation along the axial direction is proposed for the unsaturated sample. Theoretical results for the demagnetising field and the time delay have been computed using this model to explain the excitation and transmission of the observed magnetostatic waves.

## ACKNOWLEDGEMENTS

It is with great pleasure that I take this opportunity to thank Dr. M. W. Gunn and Dr. C. K. Campbell for their continued guidance and encouragement throughout this thesis project. I am especially indebted to Dr. Campbell for the many hours he spent with me during the experimental work, and to Dr. Gunn for a very critical and helpful criticism of the manuscript of this thesis.

I am very grateful to my parents for their sacrifice and encouragement all through my academic career.

My thanks are also due to Canadian Westinghouse for making available a Research Grant to carry out this project.

And finally, my thanks go to Miss Earlene Robinson for typing this thesis at such short notice.

TABLE OF CONTENTS

# CHAPTER I

# INTRODUCTION

## 1.1 Growth of Microwave Ultrasonics

Microwave ultrasonics has aroused considerable interest in the past decade, owing to:

(i) Successful development of high frequency transducers

(ii) Development of techniques for growing crystals of piezoelectric material and low-loss magnetic material.

(iii) Its importance and application in the development of microwave frequency radar and communication systems: data processing and instrumentation.

(iv) Its importance in the study of Solid State Transport. Phenomena.

## 1.2 Two Kinds of Waves

Microwave ultrasonic processes can be associated with two types of waves, namely:

a. Elastic Waves

b. Magnetic Waves

### Elastic Wave

Elastic waves propagate as vibrations of the crystal lattice at about 5 orders of magnitude less than the speed of light. Associated wave-length parameters are thus of the order of microns. Such vibrations may be described in terms of phonons or quantum elements of lattice vibration which are characterised in terms of an energy parameter $h\nu$ (h: Planck's constant; $\nu$: frequency of vibration) and a wave vector k.

Magnetic Waves

Certain magnetic insulating crystals can support and propagate pure magnetic modes or magnetostatic waves ( $10 < k < 10^{5}$ $cm.^{-1}$ where $k=2\pi/\lambda$ is the wave number) or spin waves ( $k > 10^{5}$ $cm.^{-1}$) quantised in terms of magnons as will be discussed in the next chapter. Many properties of these waves are similar to those of elastic waves; in addition, their velocity of propagation can be controlled by an appied dc magnetic field. Magnetic waves can have a velocity, an order of magnitude, less than the velocity of phonons. Magnetostatic waves travel with nearly electromagnetic speeds to very low values near the critical field; whereas, spin waves do not revert to electromagnetic speeds at low values of the field. This means that magnetostatic waves will show delays from nanoseconds to microseconds; the spin wave will have a minimum delay of several microseconds.

Magnetoelastic Waves

If the applied magnetic field is adjusted so that the wave-length associated with a particular frequency of excitation is the same as for an elastic wave of that frequency, then the magnetic and elastic waves are strongly coupled giving rise to a mode of propagation which is partly elastic and partly magnetic. Such a wave is called a magnetoelastic wave.

As described, lower velocity of propagation of elastic or magnetic waves at microwave frequencies makes their wave-length comparable with that of light; consequently many types of interactions result, e.g.;

a. Ultrasonic phonon interaction with electrons and thermal phonons yields information about the structure of solids, semiconductors or metals[1,2*]. Such interactions can be utilised for amplifications of ultrasonic waves.

b. Light interaction with microwave sound has been given a great impetus owing to the availability of coherent light from a laser. In the past, this phenomenon was utilised to determine the elastic constants of the material; but presently, research is directed to obtain better and better parametric amplification and oscillation[3].

c. High frequency acoustic waves interact with nuclear spins yielding information about the coupling of nuclear spins with lattice vibrations in solids[4].

## 1.3 Propagation and Attenuation Effects in Solids

For signal frequencies in the megacycle range, the attenuation of a propagating wave becomes prohibitivly large at room temperatures. For example, in quartz, above 40°K the absorption is almost independent of temperature; it increases with the square of the frequency, reaching very high values in the microwave region e.g. 25 to 30 db/cm

* Numbers refer to the Bibliography listing.

at 2.6 Gc/s at room temperature[5]. Below 40°K, absorption rapidly disappears even for the highest frequencies, e.g. .01 db/cm at liquid Helium temperature and at 2.6 Gs/s. The explanation of this behaviour is provided by A. I. Akhiezer[6].

Scattering is produced by the numerous microscopic defects, such as grain boundaries, dislocations, or the volume disorder. With increased frequency, the wave-length of ultrasonic waves becomes comparable with microscopic defects, with a consequent increased scattering. Better crystal growth and use of single crystals largely overcomes this effect. Flatness and parallelism, and the proper choice of orientation of the propagating medium, strongly influence the propagation and attenuation characteristics of ultrasonic waves.

## 1.4 Material Requirements

The extremely small wave-length, of the order of a few microns, associated with microwave phonons and magnons requires the material to be free of discontinuities larger than a few microns. This restricts microwave phonon and magnon propagation essentially to single crystals, which are in general very hard to grow. In addition, all end surfaces have to be plane and parallel to an optical quality to reduce scattering. For phase coherence to 1/10 wave-length of sound, a 1 cm. diameter rod operated at 3 Gc. will require a long-range flatness of $10^{-5}$cm. and parallelism between the polished faces within 2 seconds of arc.

Recent developments make Yttrium Iron Garnet an attractive material in this field. Magnetic waves can be launched, transmitted and detected in the interior of the material making optically flat and parallel faces unnecessary. The transmission losses in gigacycle range are moderate even at room temperatures ( $\simeq$ 1 db/cm.). Since YIG is ferrimagnetic, there is no bond problem. However, there is one difficulty associated with YIG, it is opaque to light. Thus it is impossible to inspect its quality by any means other than microwave acoustic propagation.

Yttrium Iron Garnet

This material $Y_3Fe_2(FeO_4)_3$ is a ferrimagnetic oxide which has a crystal structure isomorphic with the classical garnet $Ca_3Fe_2(SiO_4)_3$. The crystal structure is very nearly cubic and contains essentially no magnetic disorder. The Fe ions, which are responsible for the magnetic moment, are all trivalent. This property of crystallographic and magnetic equivalence prevents the small electrical conductivity experienced in ferrites by means of the exchange of electrons among $Fe^{2}$ and $Fe^{3}$ ions and results in a superiority over ferrites[7]. $Y_3$ is a non-magnetic trivalent ion. There are no unpaired spins, consequently $Y_3$ has no permanent spin magnetic moment. The growth of a single crystal of YIG by Nielson[8] stimulated research in fundamental experiments including magnetic propagation of microwaves.

## 1.5 Generation and Detection - Transducers

The main difficulty in converting electromagnetic energy to microwave acoustic energy is that of matching the wave-length in the cm range to the very short microwave acoustic waves having wave-lengths of a few microns. The coupling efficiency is an important consideration if the insertion loss at microwave frequencies is to be held to a minimum. Thus, very thin plates or films are required for efficient transducer action. Thin plates have been used at fundamental frequencies as high as 300 Mc/s, but beyond this they become extremely difficult to fabricate and are very fragile. Their efficiency is relativly low ($10^{-3}$ at microwave frequencies).

Other techniques developed in the past decade are:

a. Piezoelectric Coupling at the free end of a quartz crystal placed in a microwave cavity[9,10]. It requires optically flat and parallel surfaces for efficient conversion and yields narrow bandwidths. Typical values at 1 Gc would be 1-2% bandwidths with a 30 db conversion loss for one transducer action.

b. Thin Film Transducers - Piezoelectric

In the region between 100 Mc/s and a few gigacycles, transducer action by thin films of piezoelectric semiconducting materials deposited on the propagating medium affords lower conversion efficiencies (20 db at 1.6 Gc/s) and larger bandwidths (30%).[11]

A thin resistive layer in a piece of conducting piezoelectric material serves as the transducer. Three types of resistive-layer transducers have been proposed, namely:

(i) Epitaxial Layer Transducer

A resistive layer is formed on a conductive substrate.

(ii) Depletion Layer Transducer

A resistive layer is the depletion region formed at a rectifying metal-to-semiconductor contact or at a p-n junction. This region is in the order of 1000 Å which makes it suitable for operation in the 10 Gc range.

(iii) The Diffusion layer Transducer

A resistive layer is formed by diffusing a compensating impurity (such as copper) a short distance into a conductive base material such as cadmium sulphide. Since the thickness can be controlled by the diffusion process, this transducer can operate at fundamental frequencies from 100 Mc/s to 1 Gc/s with conversion losses from 7 db to 28 db and with 15% bandwidth[12].

(iv) Evaporated Layer Transducer

This transducer type, introduced in 1963 [11], consists of a vacuum-evaporated film of cadmium sulphide deposited directly onto a metal film on the ultrasonic medium. Operation in the frequency range from 100 Mc/s to about 2 Gc/s is achieved with a transducer loss of 6 db at 300 Mc/s and 15 db at 1.6 Gc/s. By careful control of deposition rate, it should be possible to deposit Cds films to resonate near 1000 Gc/s.

c. Phonon Generation by Magnetic Films

Ferromagnetic resonance of thin magnetostrictive metal films deposited on an ultrasonic medium may be utilised for transducer action. The films are subjected to a static dc magnetic field biassed for resonant mode selection. Such films, (which are easy to prepare and do not require acoustic bonding to the transmission medium), operate in the Gc/s range. Conversion efficiencies are low ( $10^{-9}$ - $10^{-10}$ at X-band [13] ) but considerable improvement may possibly be achieved with the aid of improved techniques.

d. Ferromagnetic and Precessional Modes

In the case of magnetic or magnetoelastic propagation, the transducer action is accomplished directly via coupling through resonance or precessional modes in the crystal material. An applied dc magnetic field makes the dipoles to precess about the equilibrium position i,e. the dc field value. The magnitude of the field determines the character of the precessing mode. The rf electromagnetic energy can be coupled to this mode when applied at an end, perpendicular to the dc magnetic field. The theory is developed in the next chapter.

YIG, which is ferrimagnetic, is the most promising single crystal grown so far and exhibits low propagation loss even at room temperature. It is capable of propagating both elastic and magnetic waves.

## CHAPTER II

## THEORETICAL ANALYSIS

### 2.1 Spin Waves

The concept of spin waves was introduced by Bloch in 1930 on a quantum mechanical basis. In any solid, the unpaired electron spins contribute to the magnetic properties of the solid. In a ferro- or ferri- magnetic medium, the exchange field between the atoms tends to align all the spin dipoles in the same direction. Under the application of a dc magnetic field H, the magnetic dipoles precess in unison or in phase about H. An rf magnetic field applied uniformly and perpendicular to the dc field H, over the whole sample, still gives a uniform precessional motion but with a larger precession angle. If the frequency of the rf magnetic field equals the natural precession frequency ( $\omega_0 = H_0 \gamma$ ), ferromagnetic resonance results and is accompanied by a large absorption of energy by the spins.

If; however, the rf field is applied at one end of the specimen, it causes some of the spins to precess with a larger precession angle than their neighbours; the internal exchange field, tending to align the dipoles, forces this precessional disturbance through the crystal in the form of a wave, called a spin wave. Spin waves are; therefore, waves of deflection of electron spins away from the ordered orientations that are characteristic in a magnetised material. The ground state corresponds to infinite wave-length (uniform precession) while for shorter wave-lengths, an exchange interaction results in additional energy.

In an infinite, lossless medium the dispersion relation for the spin waves in the absence of propagation effects is given by[14]: (see appendix 1)

$$\left(\frac{\omega}{\gamma}\right)^2 = \left[Hi + Dk^2\right]\left[Hi + Dk^2 + 4\pi M(k_x^2 + k_y^2)\ /k^2\right] \tag{2-1}$$

Here: $\gamma$ : gyromagnetic ratio

$1.76\ 10^7$ radians /(second) (oersted)

D : a phenomenological exchange constant, nearly equal to: $5\ 10^{-9}$ Oe.cm$^2$ for YIG.

M : saturation magnetisation

H : internal dc magnetic field, applied along the z direction

$$k^2 = k_x^2 + k_y^2 + k_z^2 \quad ;$$

where k is the spin wave number.

The last term in the relation arises from the dipolar interaction between the spins. In deriving the equation (2-1) it was implicitly assumed that the dimension of the sample is considerably larger than the wave-length of the spin wave, i.e., larger at least by a factor of 10. For larger wave-lengths, the effect of boundaries becomes significant.

## 2.2 Excitation of Spin Waves

The fundamental difficulty in coupling an electromagnetic field to spin waves is that the wave-length of the former (cm range) is much larger than the latter (micron range). The rf dipole moment of a spin wave, which could give rise to such a coupling, averages out to near zero when the sample is many wave-lengths long. To overcome this difficulty, Schlomann[15] proposed the existence of a non-uniform dc magnetic field inside the sample with a configuration such that the effective wave-length of the spin waves becomes much larger nearer the surface of the sample than it is in the interior. As a consequence, the spin waves have a localised rf dipole moment in the region where the effective wave-length is large. Coupling takes place relatively efficiently in this region and the spin wave travels in the direction of decreasing magnetic field [illegible] with changing wave-length and velocity.

## 2.3 Exchange Dominated Mode

In the exchange dominated mode of operation, the last term of Eq. (2-1) is negligible and the square of the effective magnon wave number is given by:

$$k_m^2(z) = \left[\frac{\omega}{\gamma} - H(z)\right] / D \qquad (2\text{-}2)$$

The subscript m distinguishes the magnon wave number from the phonon wave number given by $k_p = \frac{\omega}{v_p}$ ; $v_p$ being the

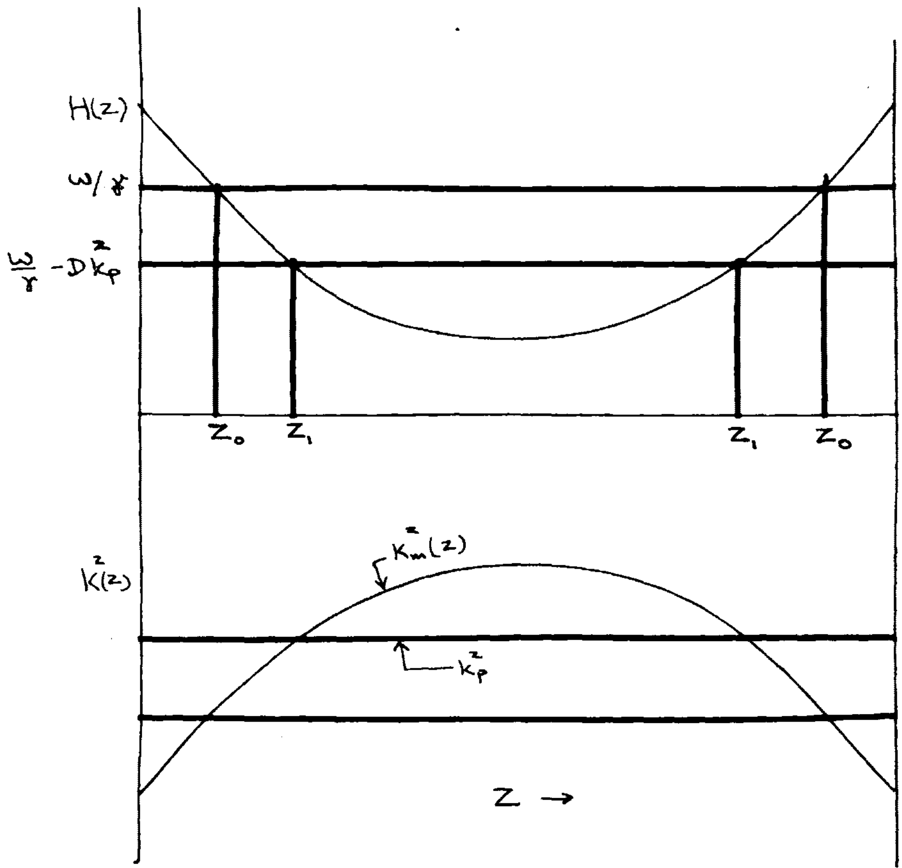


FIGURE (2-1) Shows the variation of magnetic field and the square of wave number in a specimen to transmit magnetic waves. $Z_0$'s are the turning points and $Z_1$'s are the cross over points.

velocity of elastic shear waves. $H(z)$ is the internal magnetic field and it is a function of the distance along the z direction, owing to the non-uniformity of dc magnetic field in the finite sample. We shall assume that the sample is a single crystal with the applied field along an easy or hard direction; so that the effect of crystaline anisotropy will, in the linear approximation, be to modify the applied field by an additive anisotropy field.

In effect;

$$H(z) = H_{ext.} + H_A + H_d(z) \qquad (2\text{-}3)$$

External field + Anisotropy field

+ Demagnetising field

The demagnetising field is determined by the geometry or shape of the sample and the magnetisation vector in the sample. Such a variation for a saturated cylindrical sample is as shown[16] in figure (2-1). The point at which $k_m^2(z)$ becomes zero is denoted as the 'turning point' $z_o$. The wavelength is a maximum at this point and the internal field has the proper value to bias a magnetic mode to resonance.

The spin wave which originates in the vicinity of the turning point, propagates through the sample in the direction of decreasing magnetic field, and is partially converted into elastic waves near the cross-over point $z_1$ where $k_p^2 = k_m^2$. Conversion depends upon the field gradient $H'$.

It is greater when the spin wave travels for a longer time over the cross-over region i.e. when the field gradient is small. The field gradient depends on the elastic and magnetic properties of the material.

## 2.4 Magnetostatic Mode

Near the vicinity of the turning point, the wavelength may acquire a large enough value, depending on the field gradient, which is comparable with the sample dimensions. Under such circumstances, the plane wave dispersion relation ceases to be useful - although still valid for Fourier components. To deal with such a case, it is necessary to solve the magnetostatic field equations:

$$\text{Curl } h = 0 \qquad (2\text{-}4)$$

$$\text{div } (h + 4\pi m) = 0 \qquad (2\text{-}5)$$

Where h and m are the rf field and magnetisation; and m is derived from a linearised equation of motion, subject to the boundary conditions of magnetostatics; viz.,

(i) That the tangential component of the rf magnetic field is continuous.

(ii) That the normal component of the induction, $b = h + 4\pi m$ is continuous.

These considerations led Fletcher and Kittel[17] to determine the dispersion relation of the magnetostatic waves in a cylinder, magnetised longitudinally. They arrived at the relation:

$$\omega = \gamma H_i + 2\pi \gamma M \left( \frac{2.405}{ka} \right)^2 \qquad (2\text{-}6)$$

Where: $a$ is the radius of the rod,

$M$ is the saturation magnetisation,

$k$ is the wave-number of the magnetostatic wave.

This relation assumes that the sample is large enough to ignore exchange, and small enough to neglect propagation. The three distinct regions [18] of wave propagation in a magnetised sample are classified as follows:

a. Magnetostatic Region

$10 < k < 10^5$ cm$^{-1}$

It is governed by the boundary conditions.

b. Exchange Dominated or Spin Wave Region

$k > 10^5$ cm$^{-1}$

It is determined by the exchange forces.

c. Electromagnetic Propagation

$k < 3$ cm$^{-1}$

It is governed by the dielectric property of the material.

# CHAPTER III

## THE COUPLING MECHANISM

### 3.1 Choice of the Coupling Mechanism

In this thesis, the main considerations for the choice of the coupling mechanism were;

(i) Rigidity of structure.

(ii) Efficient coupling.

(iii) Capability of being oriented precisely in the field of an electromagnet when set up in a suitable mount.

(iv) A structure in which the fragile crystal of YIG can be placed with little risk of damaging it.

(v) Flexibility of the coupling parameters.

(vi) Cheapness in cost, ease of fabrication, and testing.

These considerations led to the design of a strip-line. Coupling and support mechanism are described in the following secton.

### 3.2 Design of the Strip-line

The planar or "Flat Strip" transmission system has fundamentally evolved from the coaxial transmission system as can be seen from the figure (3-1).

The dominant mode in a balanced strip-line is a TEM mode so that the field distribution can be determined rigorously by conformal mapping.

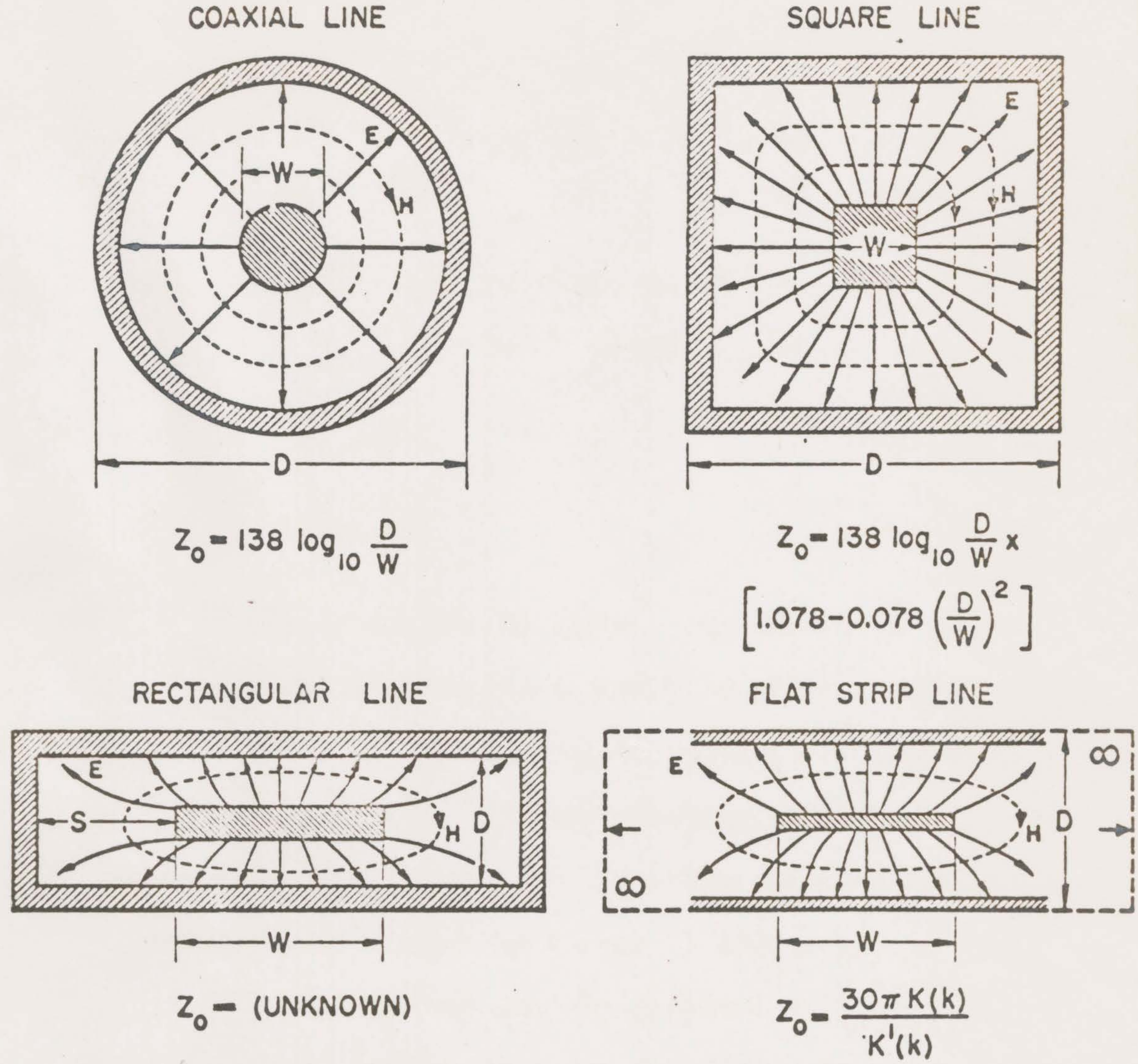


EVOLUTION OF FLAT STRIP TRANSMISSION LINE

FIGURE (3-1)

The characteristic impedence for a zero thickness, perfectly conducting inner strip air filled line, is given by the following exact formula[20]:

$$z_0 = 30\pi \frac{k(k)}{k(k')} \qquad (3\text{-}1)$$

Where: $k(k)$ and $k(k')$ are complete elliptical integrals of the first kind, and:

$$k = \operatorname{sech} \frac{\pi W}{2b} \qquad (3\text{-}2)$$

$$k' = \tanh \frac{\pi W}{2b} \qquad (3\text{-}3)$$

A family of curves, computed by Cohn[21] are shown in figures (3-2) and (3-3) with dimensions W and b as shown. The values shown are exact for $\frac{t}{b} = 0$ and are accurate to within about 1% for other values of $\frac{t}{b}$. The attenuation arising from copper and dielectric losses is a fraction of a db at 1 Gc. This loss is negligible when compared to the coupling loss; and hence, its consideration may be ignored in the design.

For this investigation, a strip-line was designed with the following characteristics:

a. A characteristic impedence close to 50 ohms.

b. A plate spacing (total thickness of the line) of magnitude roughly equal to the length of the crystal, i.e. 0.4 inches.

GRAPH OF Zo VERSUS W/b FOR VARIOUS VALUES OF t/b

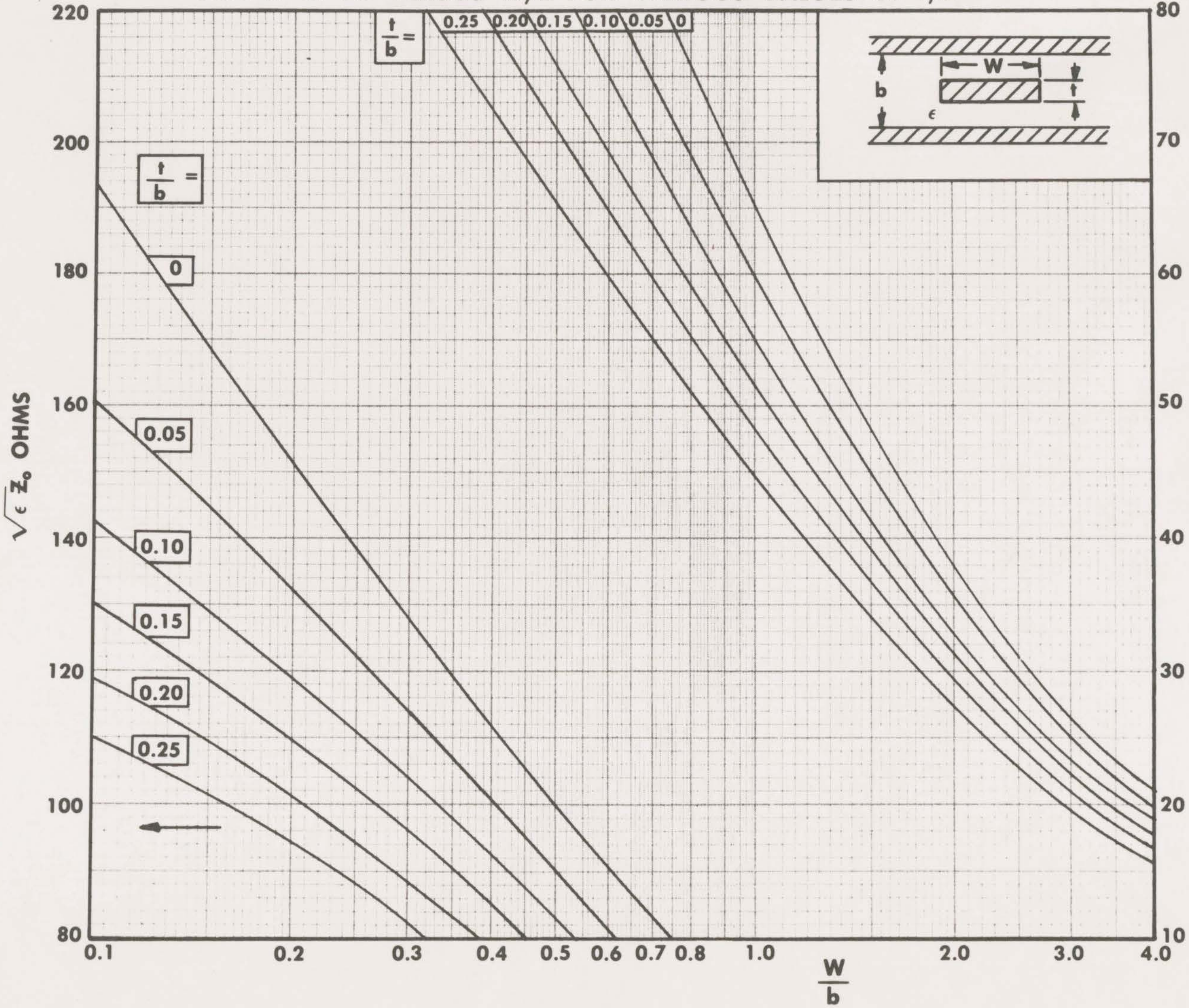


FIGURE (3-2)

c. Provision of a good short at the end of the line to provide a large rf magnetic field for efficient coupling.

### 3.3 Construction of the Strip-line

The designed description of the strip-line is shown in figures (3-2) and (3-3); the components are shown in figure (3-4). The dielectric material used is a polystyrene sheet of thickness 1/8 inch, with a dielectric constant of 2.54.

For a line impedence $z_0 = 50$ ohms, the dimensions W and t for the given b = 0.25 inch are determined from the design curves given in figure (3-2) as follows:

$$\sqrt{\epsilon_r}\ Z_0 = 50\sqrt{\epsilon_r} = \sqrt{2.54} \times 50$$
$$= 80 \text{ ohms}$$

Taking W = .04 inch

$$\frac{W}{b} = 0.16$$

and the curves give

$$\frac{t}{b} = 0.4 \quad \text{for} \qquad z_0 = 80$$

$$\therefore\ t = 0.1 \text{ inch or } 100 \text{ thou.}$$

The width and thickness of the center conductor can be varied, keeping the characteristic impedence at 50 ohms.

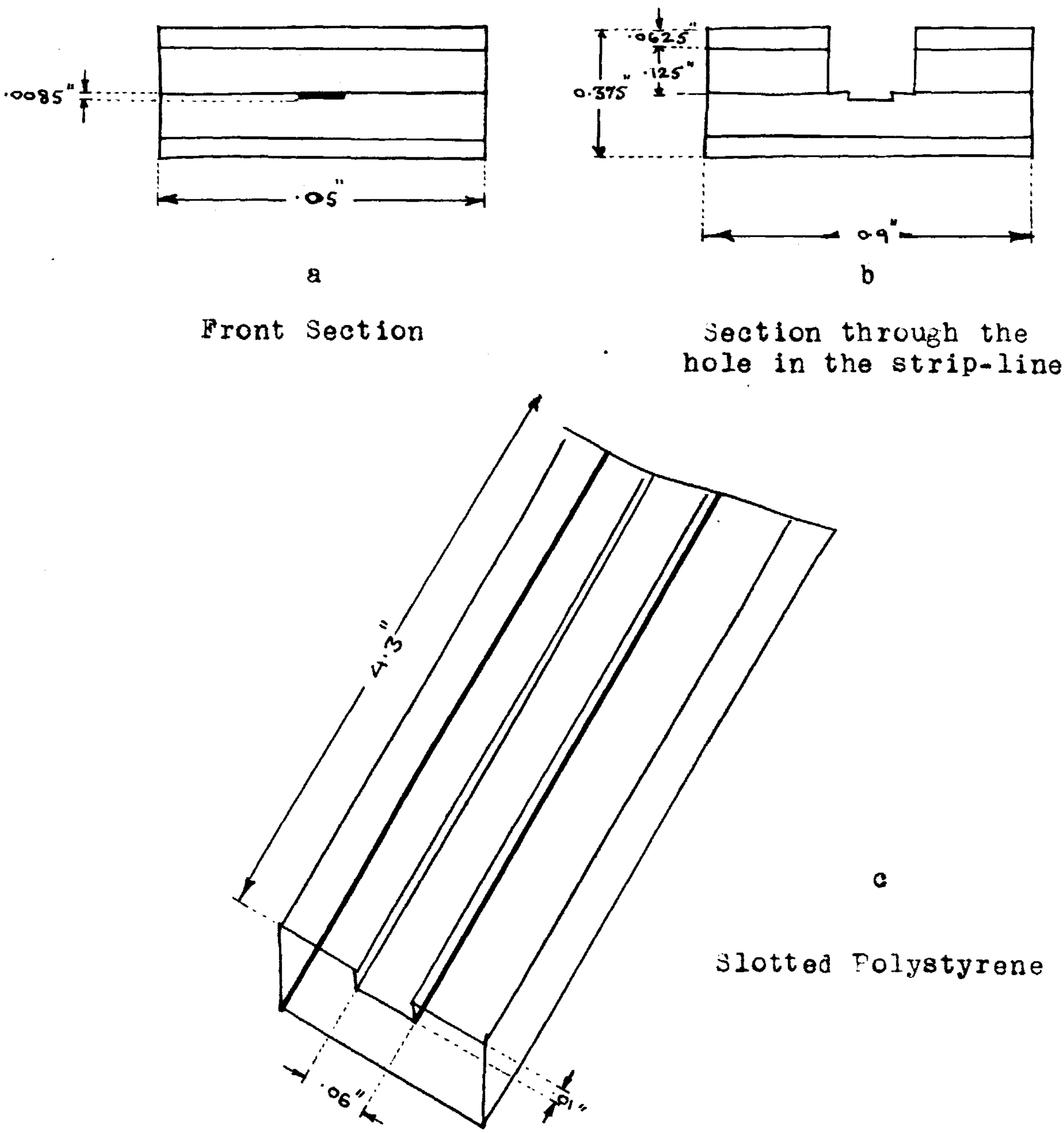


FIGURE (3-3) Designed Description of the Strip-line

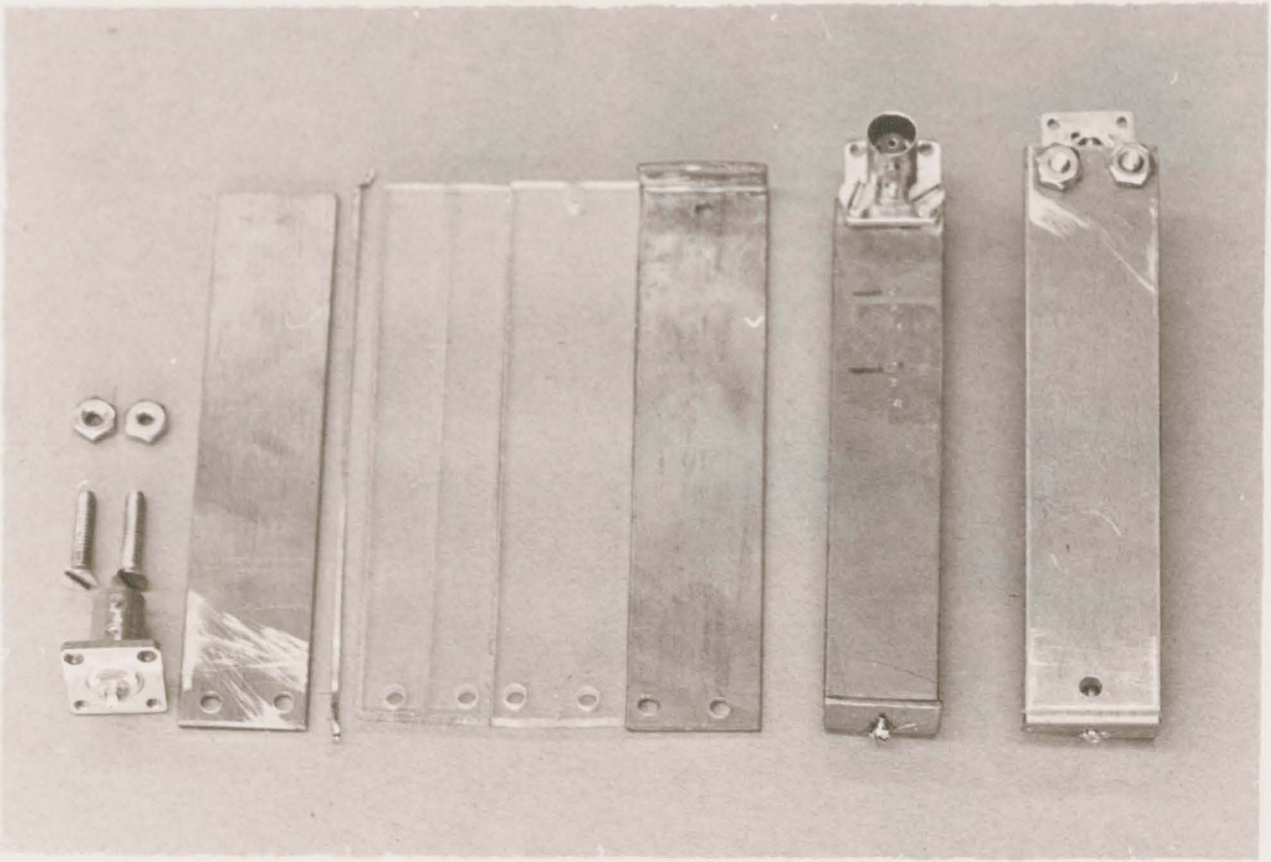

Components of the Strip-line.

FIGURE (3-4)

A limitation is imposed by the difficulty of pressing copper uniformly to the thickness of a few thou and then cutting a uniform strip from it a few thou wide. The parameters chosen for the line used in experimental work are shown in figures (3-2), (3-3) and (3-4).

A UG 290/U type connector was installed on one end of the strip-line while the other end was shorted by bending one of the outer conductors. The inner strip was shorted to the outer conductors at the end of the line by drilling a small hole in the bent outer conductor, and soldering the inner strip on it.

For the mounting of the crystal, a hole with a diameter a few thou larger than 1/8 inch (which is the diameter of the crystal) was drilled through the outer conductor and insulator on one side of the line, about 50 thou from the shorted end. Two such identical lines with a polyethylene sheet 25 thou thick between them held the crystal firmly. The center conductor was installed in a slot drilled in the center of one of the polystyrene sheets as shown in figure (3-3).

## 3.4 Testing of the Line

A block diagram is shown in figure (3-5). To determine the characteristic impedence, the line was terminated in a 50 ohm load with the short removed.

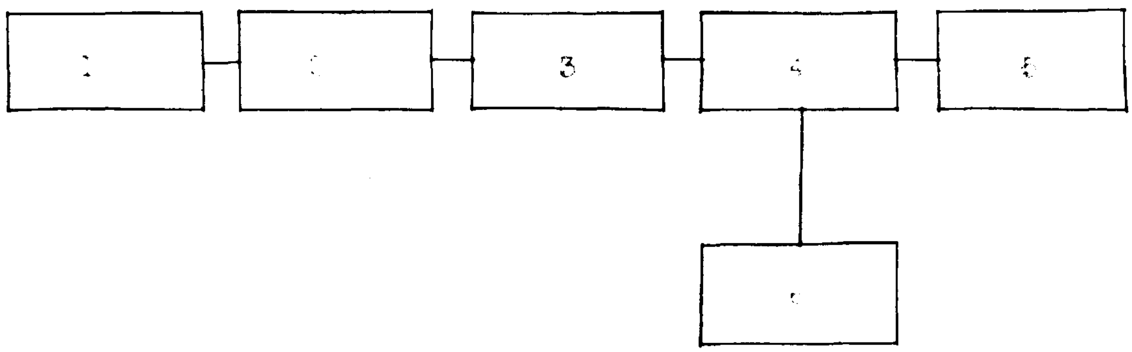


1. Modulating Power Supply
2. Unit Oscillator
3. Low Pass Filter
4. Slotted Line
5. Strip-line Terminated in a 50 Ohm Load
6. Standing Wave Indicator

FIGURE (3-5) Block Diagram for Testing the Strip-line

The voltage standing wave ratio was found to be less than 1.1 at 950 Mc/s.

### 3.5 Coupling of Electromagnetic Energy to the Crystal

The shorted end gives a current maxima i.e. rf magnetic field is maximum near the hole and parallel across the face of the crystal. The length of the line was made roughly equal to 10 cm, (in polystyrene, $\epsilon_r = 2.54$ and $\frac{\lambda}{2} \simeq$ 10 cm in the 890 - 990 Mc/s frequency range) to obtain a maximum absorption of energy. A single stub was connected to the input line to match the energy into the line. The distance between the center of the matching stub and center conductor of the line was 10 cm.

Energy is coupled out in a similar way, by the shorted center conductor of the second line facing the other end of the crystal. Output energy, generated at the shorted end sees the characteristic impedence of the line as it propagates through it; consequently, it requires no matching stub at the output end.

# CHAPTER IV

## DESCRIPTION OF APPARATUS AND MEASUREMENT

The main aim was to observe and measure the propagation characteristics of the magnetostatic waves through the YIG crystal. This involved a study of the time delay and dispersion characteristics and the associated losses as a function of the dc magnetic field.

### 4.1 Apparatus Description

The apparatus was constructed of General Radio Company's coaxial line equipment. A schematic block diagram of the complete circuit is shown in figure (4-1) with the description as follows:

a. Unit Pulser

| | |
|---|---|
| Type No. | : 1217-A, General Radio Company. |
| Time Scale (Duration) | : 0.2 $\mu$sec to 60 msec/cm. |
| Pulse Repetition Frequency | : 30 c/s to 100 k c/s. |
| Output | : 25 volts positive or negative |
| Power Supply Attached | : 1203-B GRC. |

About 0.5 sec positive pulse of repetition rate 1 or 2 k c/s was fed to the modulating power supply 1264-A as an external modulating signal.

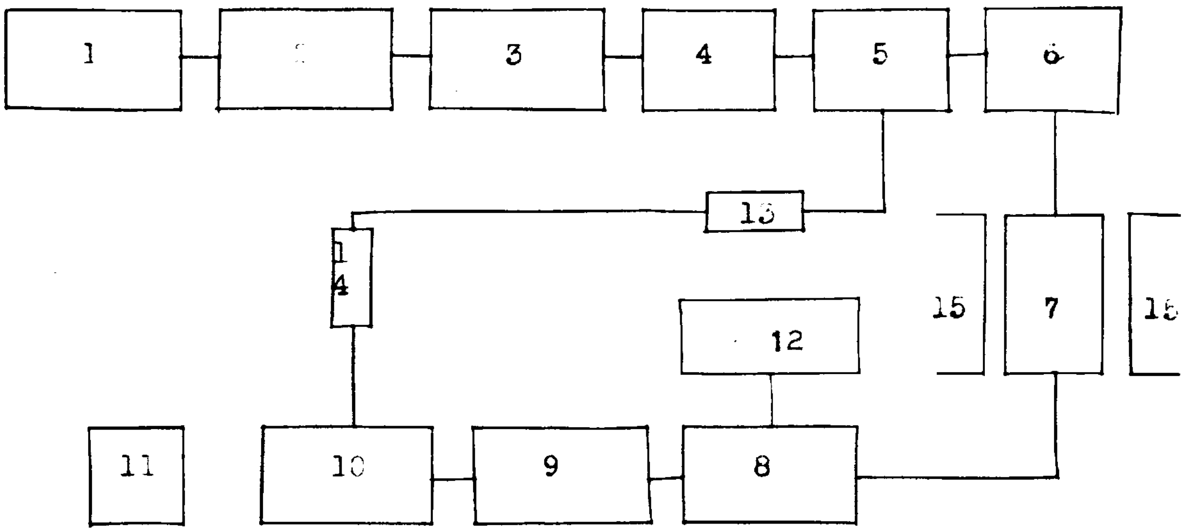


1. Unit Pulser
2. Modulating Power Supply
3. Unit Oscillator
4. Low Pass Filter
5. Voltmeter Detector
6. Variable Attenuator
7. Coupling Assembly
8. Mixer Rectifier
9. I. F. Amplifier
10. Tektronix Oscilloscope
11. Oscillotracer
12. Local Oscillator
13. T-section - one end terminated in a 50 ohm load
14. T-section - one end available for the display of input waveform
15. Pole-Pieces of the Electromagnet

FIGURE (4-1) Block Diagram of the Complete Assembly

b. Modulating Power Supply

Type No. : 1264-A GRC.

Modulation Used : External

Output : 160 - 210 volts, negative.

Rise and Decay Time : ( 10% - 90% ).

It is less than 1.5 $\mu$sec when driving a load capacitance of 300 pf in shunt with a resistance of 15 kiloohms. A modulating input pulse of about 200 volts and negative polarity was fed to the U.H.F. unit oscillator.

c. Unit Oscillator

Type No. : 1218-A GRC.

Frequency : 900 - 2,000 Mc/s.

Tuned Circuit : Adjustable lines

Calibration Accuracy : 1%

Output : About 150 mw in a 50 ohms load.

The output pulse of 990 Mc/s or less from the oscillator is passed through a low-pass filter of 100 Mc. Type 874-F 1000 GRC, Tschebyscheff type. The filtered output goes into a detector.

d. Detector and Variable Attenuator

(i) Type 874-VQ Voltmeter Detector

It introduces no appreciable discontinuity when inserted in a 50 ohm coaxial line.

Frequency Range as Matched Detector:

0.5 Mc to 2 Gc.

Resonant Frequency : About 5.4 Gc.

Maximum Voltage : :2 volts

VSWR : 1.1 at 1 Gc.

Crystal : 1N23 B

Bypass Capacitance : About 300 pf.

The detected output serves as the triggering pulse to the Oscilloscope for synchronisation, after it is passed through a T-section terminated in a 50 ohm load. A variable attenuator is connected as the load to the detector.

(ii) Type 874 - GAL Variable Attenuator

This is a waveguide-below-cutoff type attenuator. Absolute attenuation is the sum of insertion loss and scale reading. It consists of a short coaxial section, one end for source and the other for load, and introduces minimum discontinuity when inserted in a 50 ohm line.

Calibrated Range = 120 db (Relative Attenuation)

Insertion Loss = 33 ± 2 db at 1 Gc with 50 ohm termination and scale set at 0 db.

18 ± 2 db with scale at -9 db.

Accuracy = 1.3% at 50 db.

The attenuator was terminated in a 50 ohm load and the output was connected to the input strip-line through a 874-D2CI matching stub.

e. Mounting for the Strip-lines

The mounting is shown in figure (4-2). It was designed and fabricated in the Engineering Workshop. The two strip-lines can be mounted by hand so that their ends (with 1/8 inch hole) approximately face each other. Strip-line #1 can then be moved precisely in the three perpendicular directions by the screws #3,4,and 5. A glass crystal (0.4 inch long; 0.13 inch diameter) cut nearly to the size of the YIG crystal was placed in the hole of the fixed line #2. Line #1 was then moved by the precision screws so that the exposed half of the crystal was covered by the hole in it. It was then moved away in the axial direction by about 1 cm by screw #3. The glass crystal was then replaced by the YIG crystal around which was a very thin plastic (about 2 thou thick) to protect its sides from the metal surface. A polyethylene sheet 25 thou thick was placed between the lines. Line #1 was then moved axially to cover the crystal. The whole operation was carried out with utmost care as the YIG crystal is brittle and its faces are parallel and polished to an optical quality. Even a slight pressure on it can be detrimental to its quality. The mount was then screwed up to an electromagnet as shown in figure (4-3), so that the dc field applied is parallel to the axis of the crystal, i.e. (100) direction. The mount is moveable about a vertical axis and the strip-

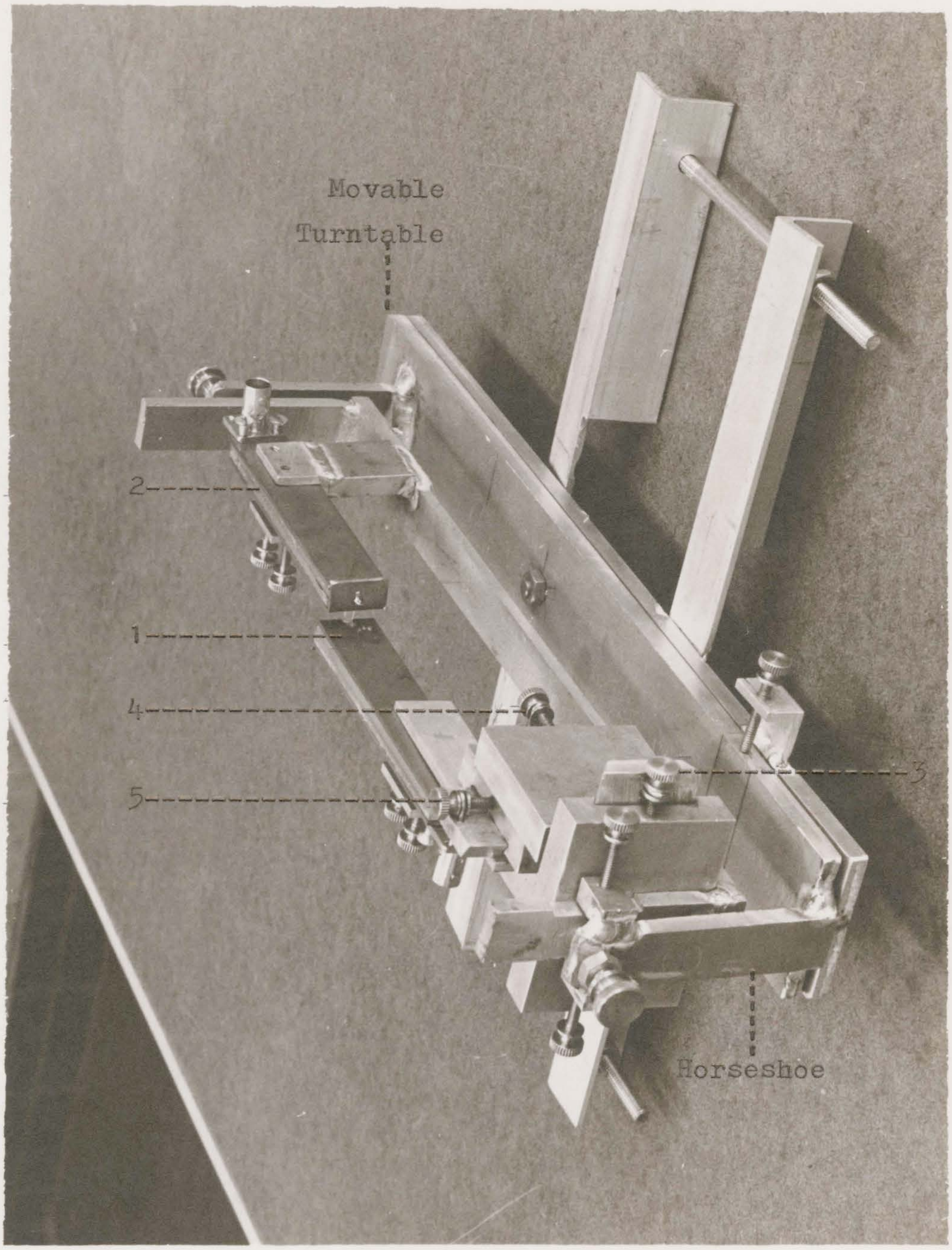


Mounting for the Strip-lines.

FIGURE (4-2)

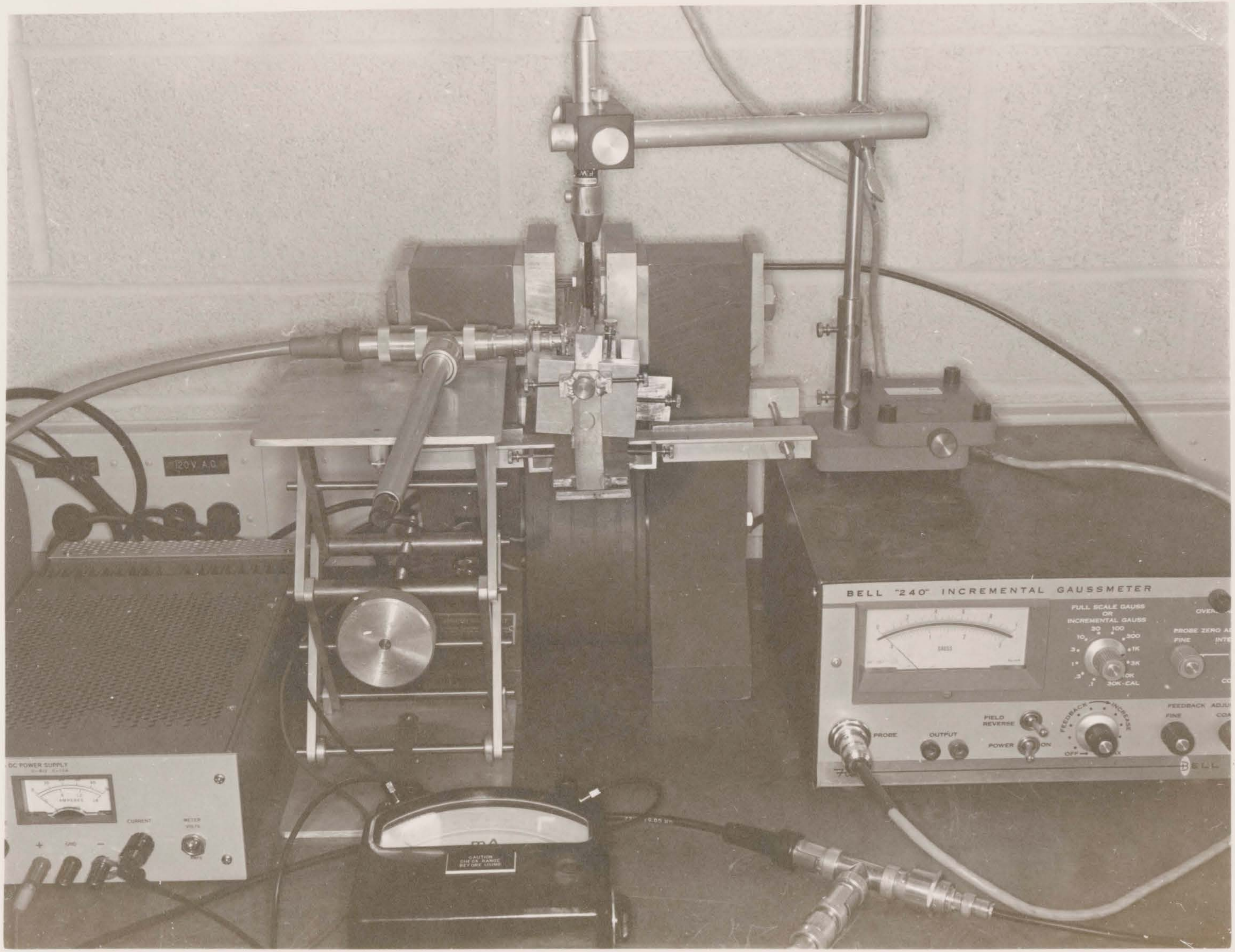


The coupling mechanism (strip-lines) clamped to the electromagnet with the mounted probe.

FIGURE (4-3)

lines along with the crystal can be swung by the horse-shoe by about $\pm 10^\circ$. This operation aligns the crystal axis with the dc magnetic field.

Power for the electromagnet was supplied by a regulated dc power supply - Harrison 6289-A. A maximum field of 1200 Oersteds could be obtained at 1.6 amperes with a gap of 1.2 inches.

The output power from strip-line #2 was fed to the signal end of the mixer described below.

f. Mixer

| | |
|---|---|
| Type No. | 874-MRL |
| Operating Frequency Range | 40 Mc to 5 Gc. |
| Crystal | 1N21 B |
| Crystal Current | 5 ma (maximum), 0.2 ma (minimum). |
| Maximum Input from Local Oscillator | 2 volts |
| Cutoff Frequency of Output Filter | 40 Mc. |
| Output Impedence | 400 ohms |

A 250 ohm series resistor isolates the signal circuit from the local oscillator.

g. Local Oscillator

| | |
|---|---|
| Type No. | 1209-B |
| Frequency Range | 250 to 960 Mc. |
| Calibration Accuracy | 1% |
| Output into 50 Ohms Load | 150 mw. |

The output is fed to the L.O. end of the mixer. It is adjusted so that the crystal current is between 0.2 ma and 5 ma, with an intermediate frequency of 30 Mc fed to an amplifier.

h. I.F. Amplifier

| | |
|---|---|
| Type : | Stagger tuned. |
| Center frequency : | 30 Mc. |
| Bandwidth : | 20 Mc. |
| Gain : | About 55 db. |
| Noise Figure : | Around 1.2 db. |
| Anode Power Supply : | Teslaa |

Filaments were heated by a 6.3v dc from Harrison 6289-A dc power supply to keep the noise to a minimum.

The output of the amplifier is fed to a built-in demodulator section which detects the initial half-micro second pulse from the 30 Mc I.F. A cathode follower section feeds the oscilloscope via a 3-foot coaxial cable.

i. Oscilloscope

| | |
|---|---|
| Type No. : | Tektronix 585 |
| Time Base : | Adjustable from .05 $\mu$sec to 2 seconds/cm. |
| Vertical Scale : | Adjustable from .01 volts to 20 volts/cm. |
| Plug-in-type Used : | Type 86 |

This incorporates a calibrated high gain

(0.1 – 20 V /cm AC/DC coupled),

fast rise time ( 1.5 nano sec) dc preamplifier. The accuracy desired (variation of delay from 0 to a few $\mu$ secs. of a 0.5 $\mu$sec. input pulse) is covered by the scope's accuracy. Figure (4-4) depicts the complete assembly.

## 4.2 Measuring Technique

The calibration accuracy of the oscillator 1218-A was checked, using a slotted line and a Standing Wave Indicator. Accuracy indicated by the curve in figure (4-5) confirms that the calibration accuracy is within 1%. The measurement of the dc magnetic field was carried out using an incremental Gaussmeter, Bell "240".

This Gaussmeter is a precision magnetic flux measuring instrument and has two main advantages:

(i) It can measure AC or DC fields from 100 milligauss to 30,000 gauss with high accuracy ( 1% ).

(ii) It can measure small changes or increments in magnetic flux density. A controlled feedback arrangement in the model makes it capable of magnifying a small change in field strength by a factor of 100.

In the 1 kilogauss range, an incremental field of 0.1 gauss could be measured on the meter. This was very helpful in studying the variation of time-delay with

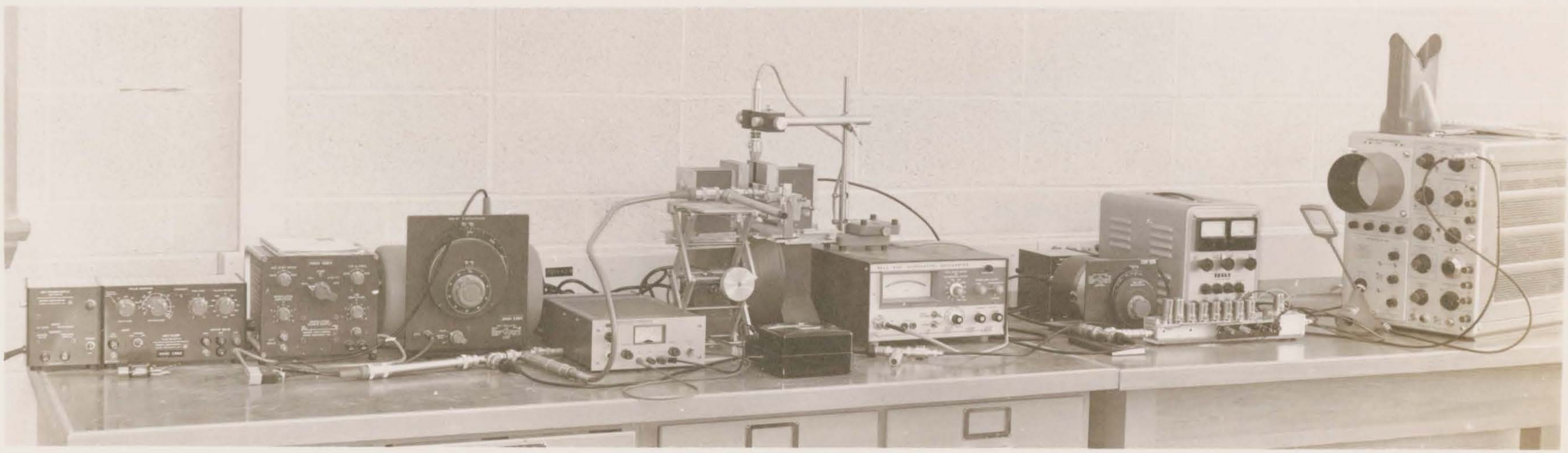

The Complete Assembly of the Equipment.

FIGURE (4-4)

Calibration Curve for the Oscillator

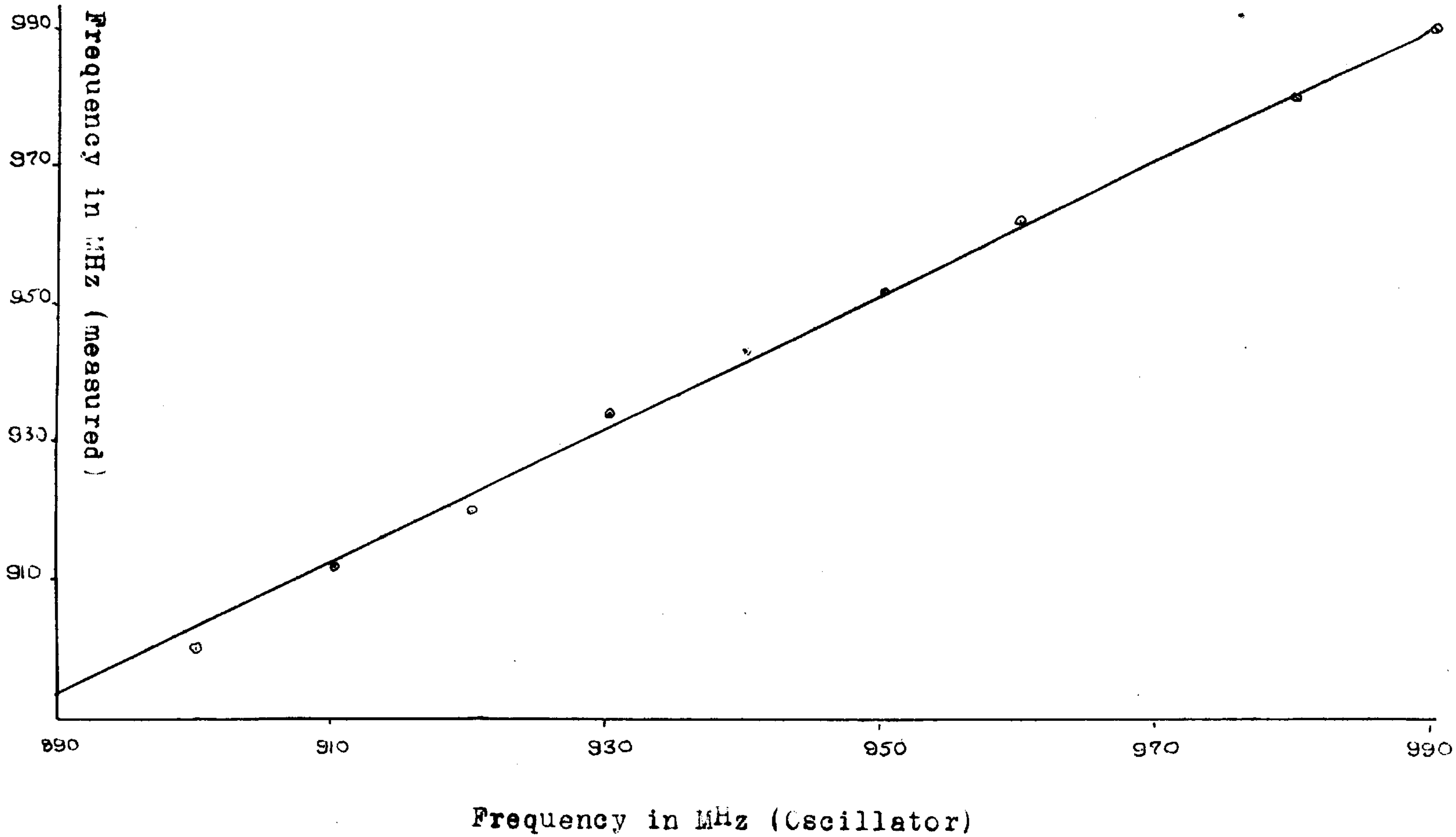


FIGURE (4-5)

FIGURE (4-5) Calibration Curve for the Oscillator increments in magnetic field near the critical field region.

The probe was mounted as shown in figure (4-3). It was adjusted to give maximum deflection in the meter. Near the critical field, feedback mechanism was operated so that a change of field up to 0.1 gauss could be measured. The probe was held in a fixed position throughout the measurements.

## 4.3 Time Delay Measurements

The input pulse was passed through a detector ( Type : 874-VQ ). The detected output was fed to a T-section and part of it was utilised to trigger the time-base of the scope and the rest was available to be displayed on the scope. The starting point of the input pulse was chosen at a well defined point, and was held at that point throughout the study of output wave forms. Magnetostatic waves were observed and were studied between the frequencies 890 to 990 Mc with a 10 Mc interval.

The quality and delay of the output pulse were optimised by aligning the crystal axis direction with the dc field, using the precision arrangements on the mounting as described earlier. The single stub before strip-line #1 was adjusted for maximum output.

An Oscillo-tracer was used to plot the waveforms as shown in figure (4-6).

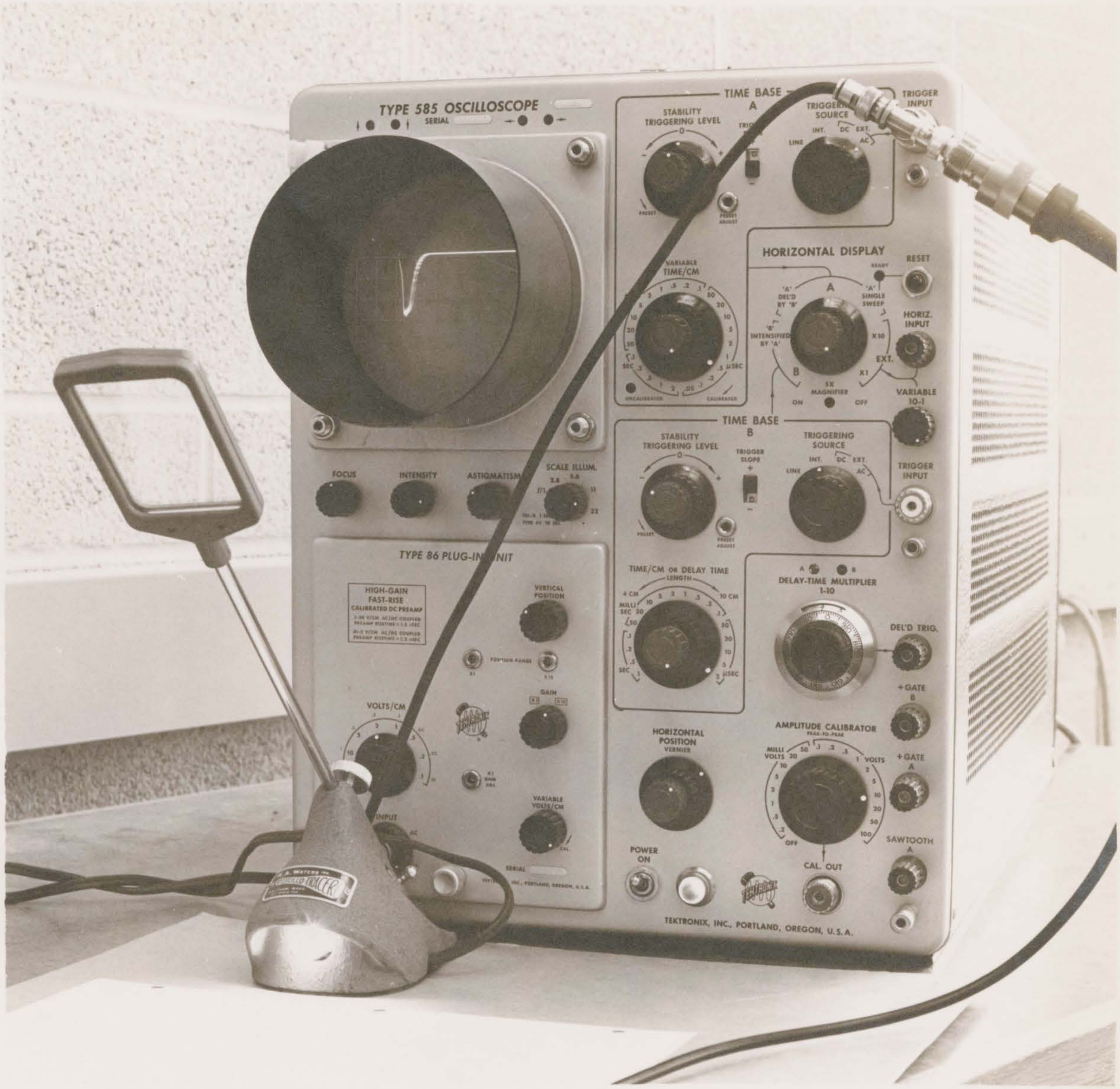


Plotting of the Waveforms Using the Oscillotracer.

FIGURE (4-6)

## 4.4 Attenuation Measurement

The insertion loss from the input end of strip-line #1 to the output end of strip-line #2 was measured by substitution method. The output pulse was observed with the variable attenuator set at the position of minimum attenuation. The coupling mechanism (comprising of the two strip-lines with the crystal in) was then removed from the circuit and the variable attenuator adjusted to yield the same output. The differance between the two attenuator readings gave the insertion loss.

## CHAPTER V

## RESULTS AND DISCUSSION

### 5.1 Results

Magnetostatic waves were observed when the externally applied dc magnetic field was in the region 460 - 515 Oersteds for the range of frequencies covered in this work i.e. 890 - 990 Mc. All measurements were carried out at room temperature.

A leakage pulse was observed at the beginning of the oscilloscope trace at all fields. Near the critical field, the transmitted pulse became observable, departing slowly from the leakage pulse at first and then sharply as the external field is increased by a few Oersteds. The increased delay is accompanied by an increased pulse width and attenuation, the delayed pulse disappearing completely before 2 microseconds delay. A typical observation is shown in figure (5-1).

The characteristics of these magnetostatic waves are analysed by plotting the curves of different parameters as shown in figures (5-2), (5-3), (5-4), (5-5), and (5-6).

### 5.2 Discussion of Results

Recalling the dispersion relation (2-6), we have:

$$\omega = \gamma H_i + 2\pi\gamma M_s \left(\frac{2.405}{Ka}\right)^2$$

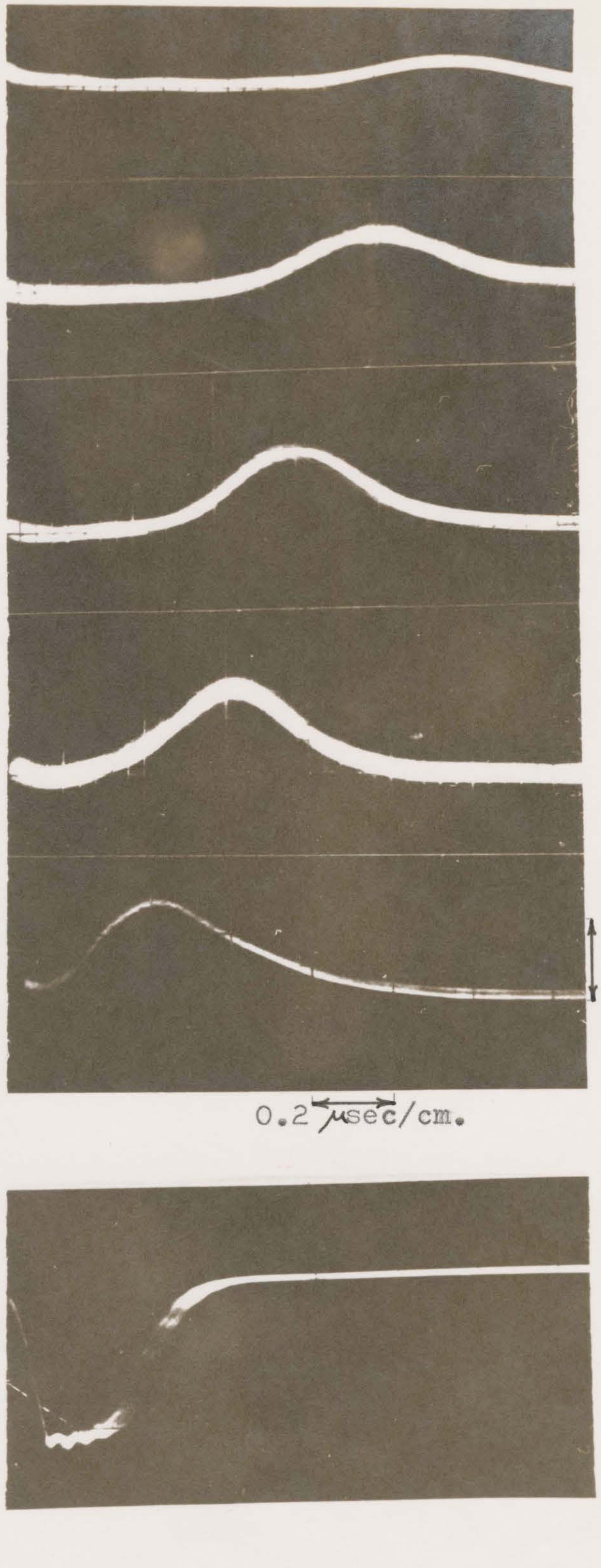


FIGURE (5-1) : Magnetostatic Waves Through the YIG Crystal
At 950 MHz

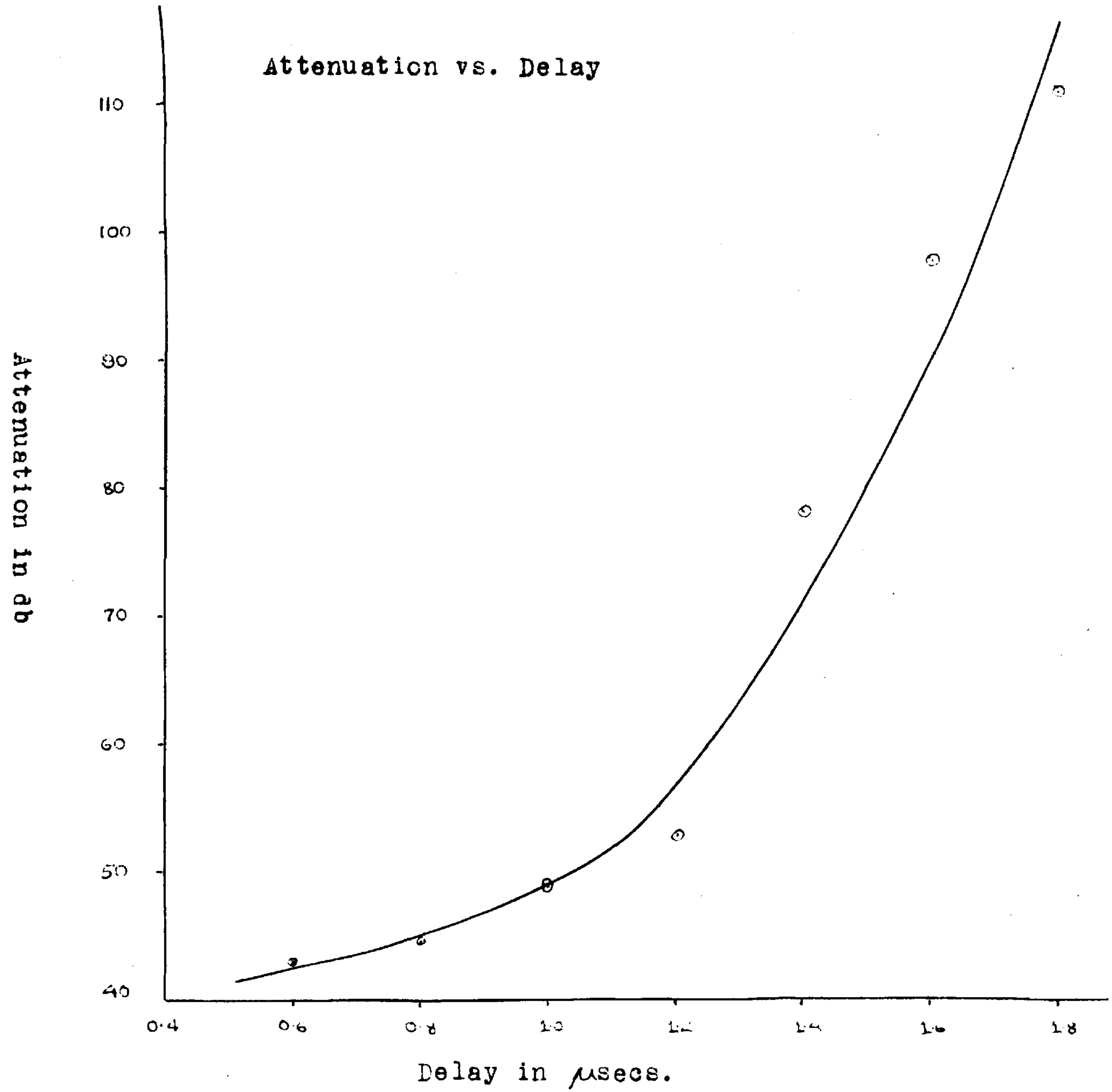
Attenuation vs. Delay
110
100
90
80
70
60
50
40
Attenuation in db
0·4
0·6
0·8
1·0
1·8
Delay in μsecs.

FIGURE (5-2)

The group velocity is given by:

$$V_g = \frac{\partial \omega}{\partial k}$$

$$= 4\pi \gamma M_s \left(\frac{2.405}{a}\right)^2 \frac{1}{k^3}$$

$$= -2 \frac{(\omega - \gamma H_i)^{3/2}}{\sqrt{2\pi \gamma M_s} \; \frac{2.405}{a}}$$

$$\text{or: } |V_g| = \frac{1.06}{10^6} (\omega - \gamma H_i)^{3/2} \qquad (5\text{-}1)$$

Hi is the internal field in the specimen given by:

$$H_i = H_{ext.} + H_a + H_d \qquad (5\text{-}2)$$

Where:

$H_{ext.}$ = Externally applied dc magnetic field

$H_a$ = Anisotropy field in the specimen

$H_d$ = Demagnetising field at the given $H_{ext.}$

Equation (5-1) implies that an increase in Hi is accompanied by a decrease of the group velocity and therefore an increase in the delay.

The generation of one or the other kind of magnetic waves depends on the frequency of operation, magnetic field developed inside the specimen, the variation of the field inside the specimen and the coupling efficiency. For magnetostatic waves, the coupling efficiency is high because of their greater wave-length and small wave number k (§ 2.5a). Therefore the delay is variable from nearly zero to a few microseconds by increasing the applied magnetic field by a few Oersteds. This was experimentally observed, confirming that the observed waves were magnetostatic. The wave number k for these waves is given by the equation (2-6), viz.:

$$\frac{1}{k^2} = (\omega - \gamma Hi) \left(\frac{a}{2.405}\right)^2 \qquad (5\text{-}3)$$

and velocity is given by (5-1).

$$Vg = \frac{1.06}{10^6} (\omega - \gamma Hi)^{3/2}$$

Where:

$$Hi = H_{ext.} + H_a + H_d$$

For a constant delay, $\omega$ varies linearly with $H_{ext.}$ if we assume that $H_d$ remains substantially constant over the frequency and dc magnetic field ranges covered. This is shown by curves in figure (5-3). The linearity of these curves implies that curves between incremental external field and incremental delays for the different frequencies used should be the same, within the experimental error. This is confirmed by the curves in figures (5-4) and (5-5). Curve in figure (5-5) is a typical (for 950 Mc) and average curve for the frequency range covered in this work.

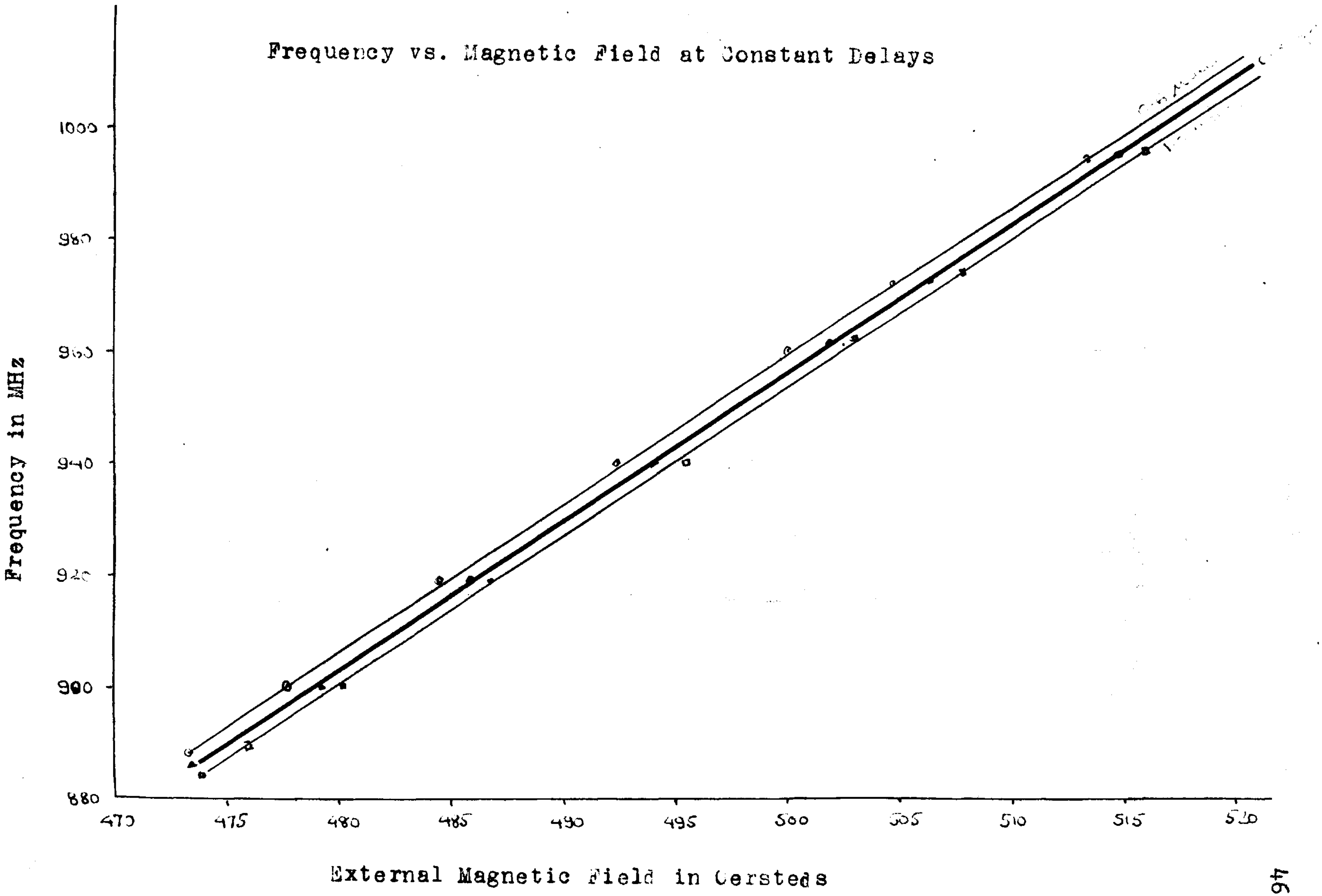
Frequency vs. Magnetic Field at Constant Delays
Frequency in MHz
1000
980
960
940
920
900
880
470
475
480
485
490
495
500
505
510
515
520
External Magnetic Field in Oersteds

FIGURE (5-3)

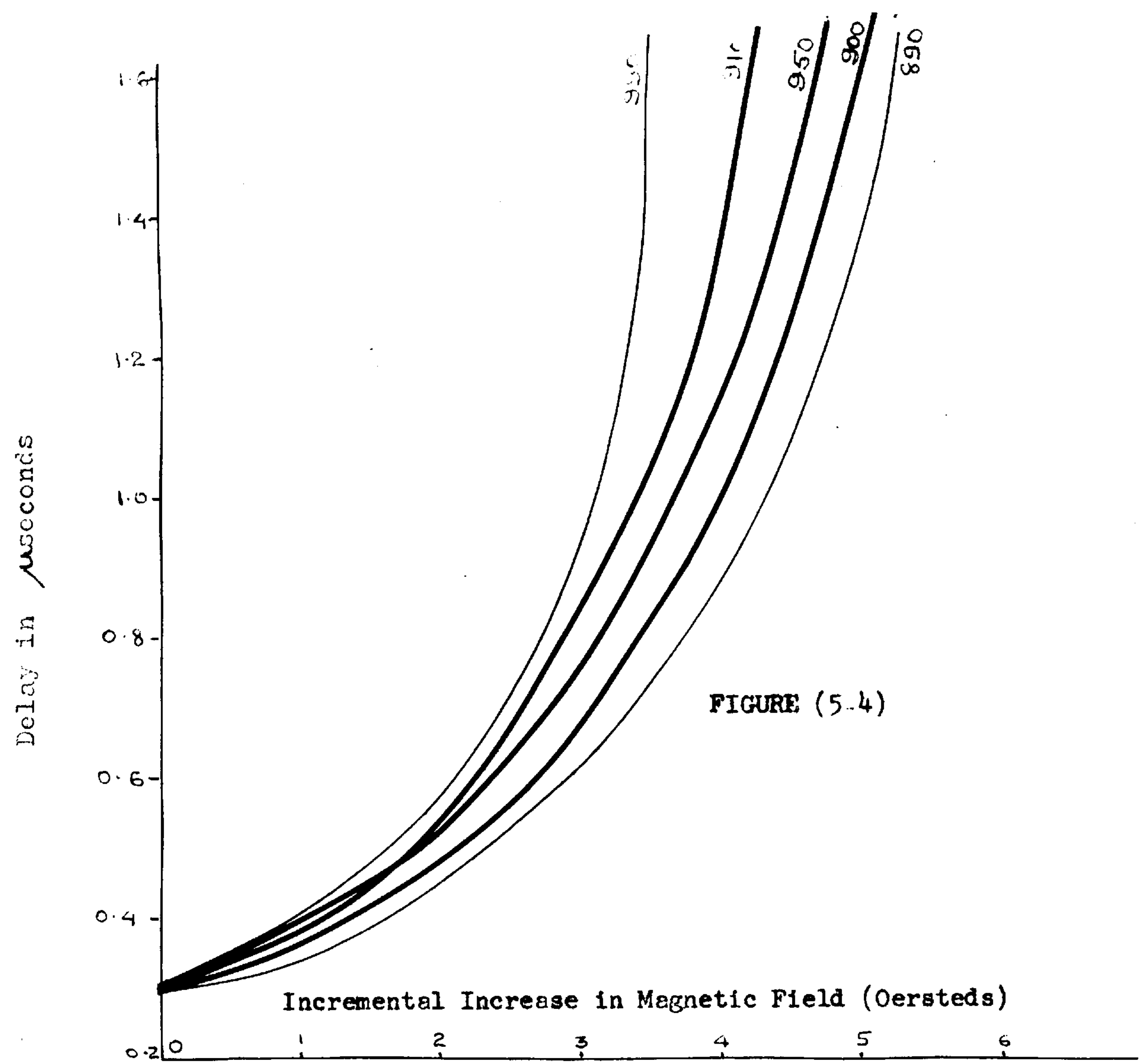


Incremental Delays vs. Incremental Fields for Different Frequencies

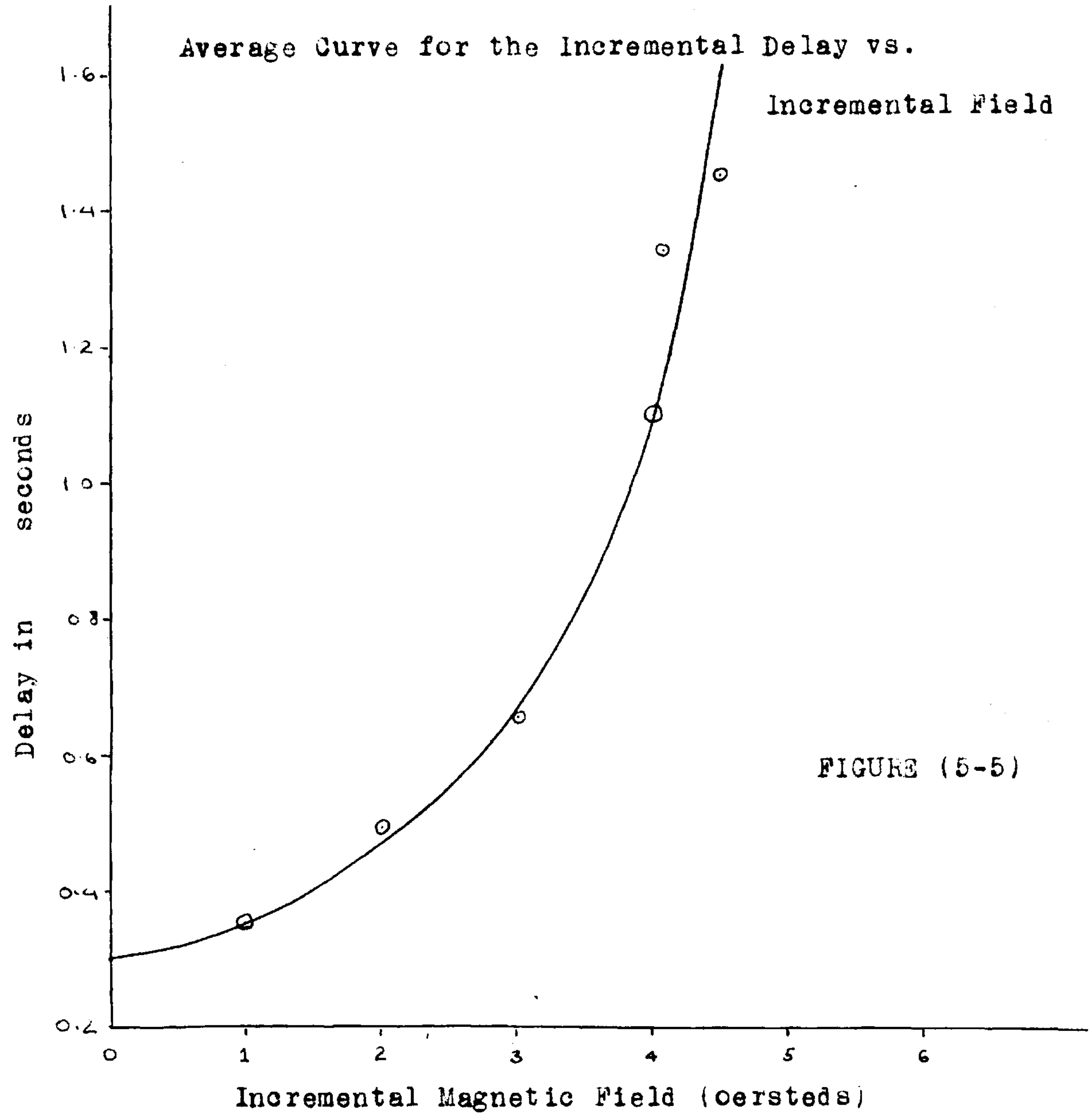

Average Curve for the Incremental Delay vs.
Incremental Field
Delay in seconds
1·6
1·4
1·2
1·0
0·8
0·6
0·4
0·2
0
1
2
3
4
5
6
Incremental Magnetic Field (oersteds)


FIGURE (5-5)

It was explained in Chapter 2 that magnetic waves are generated in the neighbourhood of the turning point where the internal field satisfies the resonance condition $Hi = \omega/\gamma$. At a given frequency, both magnetostatic and exchange dominated spin wave modes exist only below the resonance field $Hi = \omega/|\gamma|$. For the magnetostatic case it may be seen from the solution of the potential function $\Psi$ given by: (see appendix 11)

$$\Psi in = Ain\ Jn \left[ ik\rho / (1 + \kappa)^{1/2} \right] \times$$

$$e^{ikz}\ e^{in\phi} \qquad (5\text{-}4)$$

with symbols as explained in the appendix.

$$\frac{\partial^2 \Psi}{\partial z^2} = -k^2(z)\ \Psi$$

$$\text{or:} \quad \frac{\partial}{\partial z}\left(\frac{\partial \Psi}{\partial z}\right) + k^2(z)\ \Psi = 0 \qquad (5\text{-}5)$$

Where $k^2(z)$ is given by (5-3). The potential function is related to the rf magnetic field (and therefore rf magnetisation) by:

$$h = -\text{grad}\ \Psi$$

Considering the z direction which is the direction of propagation, we see that the rate of change of the slope $\frac{\partial \Psi}{\partial z}$ is $-k^2(z)$. For $k^2 < 0$, rate of change of slope has the same sign as $\Psi$ (or rf magnetisation). Consequently it never goes through zero as z is increased and the wave function decays exponentially. $\Psi$ approaches zero monotonically as z goes to infinity. On the other hand, if $k^2 > 0$, the solution of the wave function is oscillatory. Thus if $\Psi > 0$, the slope always decreases as z increases, eventually going through zero; when $\Psi < 0$, the rate of change of slope is positive so that $\Psi$ goes through zero again and becomes positive and another cycle starts. This shows that magnetostatic waves propagate when $k^2 > 0$ and since from equation (5-3)

$$\frac{1}{k^2} = ( w - \gamma H_i ) (a / 2.405 )^2$$

this implies that for propagating waves $(w/\gamma - H)$ should be positive i.e. magnetostatic waves travel in the region where the internal magnetic field is below the value $w/\gamma$ . The roots of the equation $w = \gamma H_i (z)$ determine the turning points.

These arguments lead one to expect a non-uniform internal magnetic field with the region of propagation below the value $w/|\gamma|$ . The device used in the experimental work was a two port type; therefore, the magnetostatic waves had to progress from one end to the other in order to be detected. Thus we should have an internal field which is in the neighbourhood of $w/\gamma$ near the ends of the rod and decreasing towards the center. That is, the shape of the curve relating $H_i$ and z should be concave.

## 5.3 Proposition of a Non-uniform Internal Magnetic Field for the Unsaturated Case

The magnetic field at which the magnetostatic waves were observed was in the neighbourhood of 500 Oersteds. This is much below the saturation value of 1750 Oersteds at room temperature and consequently we cannot assume that the magnetisation M is uniformly distributed in the sample and pointing in the direction of the external field.

Strauss has made use of Sommerfield's relation for the demagnetising field along the axis of a uniformly axially magnetised cylinder, viz:

$$H_d = 2\pi M_s \left[ \frac{l-z}{\left\{(l-z)^2 + a^2\right\}^{1/2}} + \frac{l+z}{\left\{(l+z)^2 + a^2\right\}^{1/2}} - 2 \right] \qquad (5\text{-}6)$$

Where:

$2l$ = Rod length

$z$ = Distance from the center of the rod

$a$ = Radius of the rod

$M_s$ = Saturation magnetisation

The external field was greater than $2\pi M_s$ so that (5-5) is a good approximation for the demagnetising field. This relationship has been arrived at from the differential equation for the potential function $\Psi$[10], i.e.

$$\Psi = -\int \frac{\operatorname{div} M}{r}\, d\tau - \int \frac{M_n}{r}\, d\sigma \qquad (5\text{-}7)$$

Mn is the normal component of magnetisation at the surface, $d\tau$ and $d\sigma$ are elemental volume and surface respectively. When we consider the magnetisation to be uniform;

$$\operatorname{div} M = 0$$

and $M_n = M_s$, the saturation magnetisation.

Under this condition, relation (5-5) gives the demagnetising field. The plot for such an internal field is depicted by the curve in figure (5-6), use being made of the IBM 7040 Computer. The programme is attached at the end. The convex shape of this curve does not explain the experimental observations, for which we require a suitable concave shape as discussed in the previous section. It is therefore proposed that the magnetisation along the z direction of the specimen is non-uniform and is described by the following equation :

$$M = \frac{M_1}{2} \left(1-\frac{z^2}{l^2}\right) + Mn \qquad (5-8)$$

This implies that the magnetisation has two components, one varying parabolically along the z direction of the sample and the other of constant value Mn. The maximum value of M is the saturation magnetisation value of 1750 Oersteds. The distribution is symmetrical about the center of the rod owing to the uniformity of the externally applied magnetic field and the structure of the specimen.

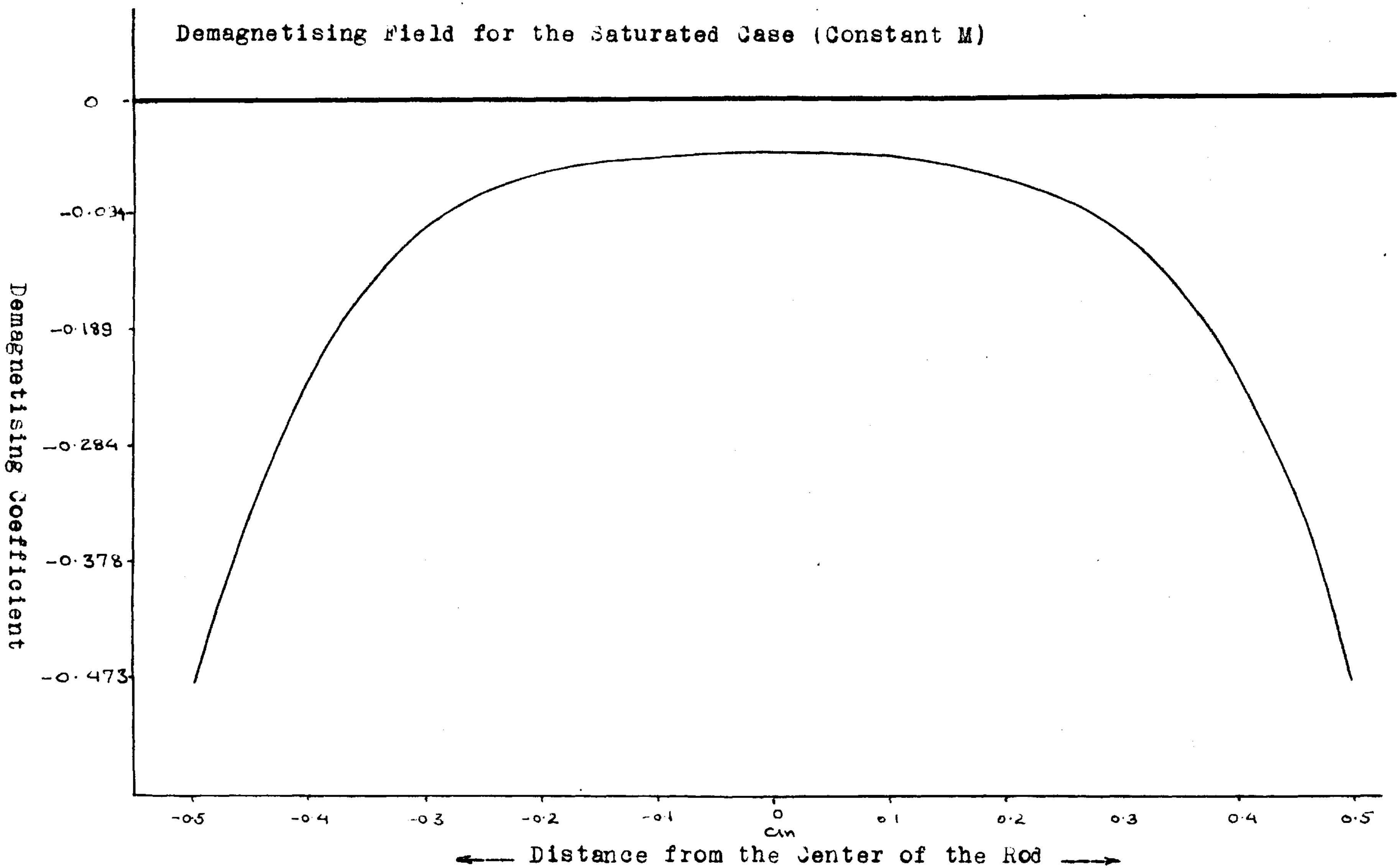
Demagnetising Field for the Saturated Case (Constant M)
0
-0.034
-0.189
-0.284
-0.378
-0.473
Demagnetising Coefficient
-0.5
-0.4
-0.3
-0.2
-0.1
0
0.1
0.2
0.3
0.4
0.5
cm
Distance from the Center of the Rod

FIGURE (5-6)

The demagnetising field is calculated from equation (5-8) in two parts, the resultant field being obtained as a superposition of the two. The constant term Mn gives a demagnetising field $H_{d1}$ as described in equation (5-6), viz.

$$H_{d1} = 2\pi\, Mn \left[ \frac{1-z}{\left\{(1-z)^2 + a^2\right\}^{1/2}} \right.$$

$$\left. + \frac{1+z}{\left\{(1+z)^2 + a^2\right\}^{1/2}} - 2 \right] \qquad (5\text{-}9)$$

The YIG specimen used in the experimental investigations had the following constants:

$2l$ = Rod length = 0.402 inch

$2a$ = Diameter of the rod = 0.125 inch

This is shown in curve (5-6). The demagnetising field owing the first term of (5-8) is as follows:

$$\operatorname{div} M = -M_1 \frac{z}{l^2}$$

With $\xi, \rho, \psi$ for the coordinates of the point of integration, and $z, p, \phi$ for the coordinates of the referance point, equation (5-6) yields:

$$4\pi \gamma = \frac{M_1}{l^2} \iiint \frac{\xi}{r}\, d\xi \; d\sigma \,, \qquad (5\text{-}10)$$

Where:

$$r^2 = (z - \xi)^2 + p^2 + \rho^2 - 2 \times p \rho \operatorname{Cos} (\phi - \psi)$$

and: $d\sigma = \rho \; d\rho \; d\psi$

On the bar axis $p = 0$ and we obtain from (5-9) by carrying out the integrations with respect to $\rho$ and $\psi$ (see appendix 111)

$$\Psi = \frac{M_1}{2l^2} \int_{-1}^{1} \xi \, d\xi \left[ \left\{ (z-\xi)^2 + a^2 \right\}^{1/2} - |z-\xi| \right] \qquad (5\text{-}11)$$

or

$$\Psi = \frac{M_1}{2l^2} \int_{-1}^{1} \xi \, d\xi \left\{ (z-\xi)^2 + a^2 \right\}^{1/2} +$$

$$\frac{M_1}{2l^2} \left( \frac{1}{3} z^3 - z\, l^2 \right)$$

$$Hd_2 = -\frac{\partial \Psi}{\partial z}$$

$$= \frac{M_1}{2l^2} \int_{-1}^{1} \xi \, d\xi \, \frac{\partial}{\partial \xi} \left\{ (z-\xi)^2 + a^2 \right\}^{1/2} +$$

$$\frac{M_1}{2l^2} (z^2 - l^2)$$

$$Hd_2 = \frac{M_1}{2l} \left[ \left\{ (z-l)^2 + a^2 \right\}^{1/2} + \left\{ (z+l)^2 + a^2 \right\}^{1/2} + \frac{z^2 - l^2}{l} \right]$$

$$- \frac{M_1}{2l^2} \int_{-1}^{1} \left| (z-\xi)^2 + a^2 \right|^{1/2} d\xi \qquad (5\text{-}12)$$

The modulus symbol || implies that the sign of this square root is to be positive. Let us consider the second term of the equation (5-12), i.e.

$$-\frac{M_1}{l^2}\int_{-l}^{l}\left|(z-\xi)^2+a^2\right|^{1/2}d\xi$$

$$=-\frac{M_1}{2l^2}\int_{-l}^{z}\left\{(z-\xi)^2+a^2\right\}^{1/2}d\xi\ -$$

$$\frac{M_1}{2l^2}\int_{z}^{l}\left\{(\xi-z)^2+a^2\right\}^{1/2}d\xi$$

$$=\frac{M_1}{2l^2}\ \frac{1}{2}\Big[2a^2\log a-(z+l)\sqrt{(z+l)^2+a^2}-(l-z)\sqrt{(l-z)^2+a^2}$$

$$-a^2\log\left\{(z+l)+\sqrt{(z+l)^2+a^2}\right\}\left\{\sqrt{(l-z)^2+a^2}+(l-z)\right\}$$

as derived in appendix 111.

Substituting in equation (5-12), we get:

$$Hd_2 = \frac{M_1}{2l}\left[\left\{(z-l)^2 + a^2\right\}^{1/2} + \left\{(z+l)^2 + a^2\right\}^{1/2} + \frac{z^2 - l^2}{l}\right]$$

$$+ \frac{M_1}{2l^2}\,\frac{1}{2}\Bigg[2a^2 \log a - (z+l)\sqrt{(z+l)^2 + a^2}$$

$$-(l-z)\sqrt{(l-z)^2 + a^2} - a^2 \log\left\{(z+l) + \sqrt{(z+l)^2 + a^2}\right\} \times$$

$$\left\{(l-z) + \sqrt{(l-z)^2 + a^2}\right\}$$

(5-13)

This field is plotted by carrying out the calculations using IBM 7040 computer, as shown by the curve in figure (5-7). This has the desired concave shape. The resultant curve for the proposed demagnetising field, equation (5-7), is obtained by superimposing the fields obtained from equations (5-9) and (5-13). The components $M_1$ and $M_n$ are chosen so that the internal magnetic field near the ends is in the neighbourhood of $\omega/\gamma_1$ and that the maximum value of $M_1$ and $M_n$ is 1750 Oersteds.

The internal field Hi is given by equation (5-2):

$$Hi = H_{ext.} + H_a + H_d$$

Where : $H_d = H_{d1} + H_{d2}$

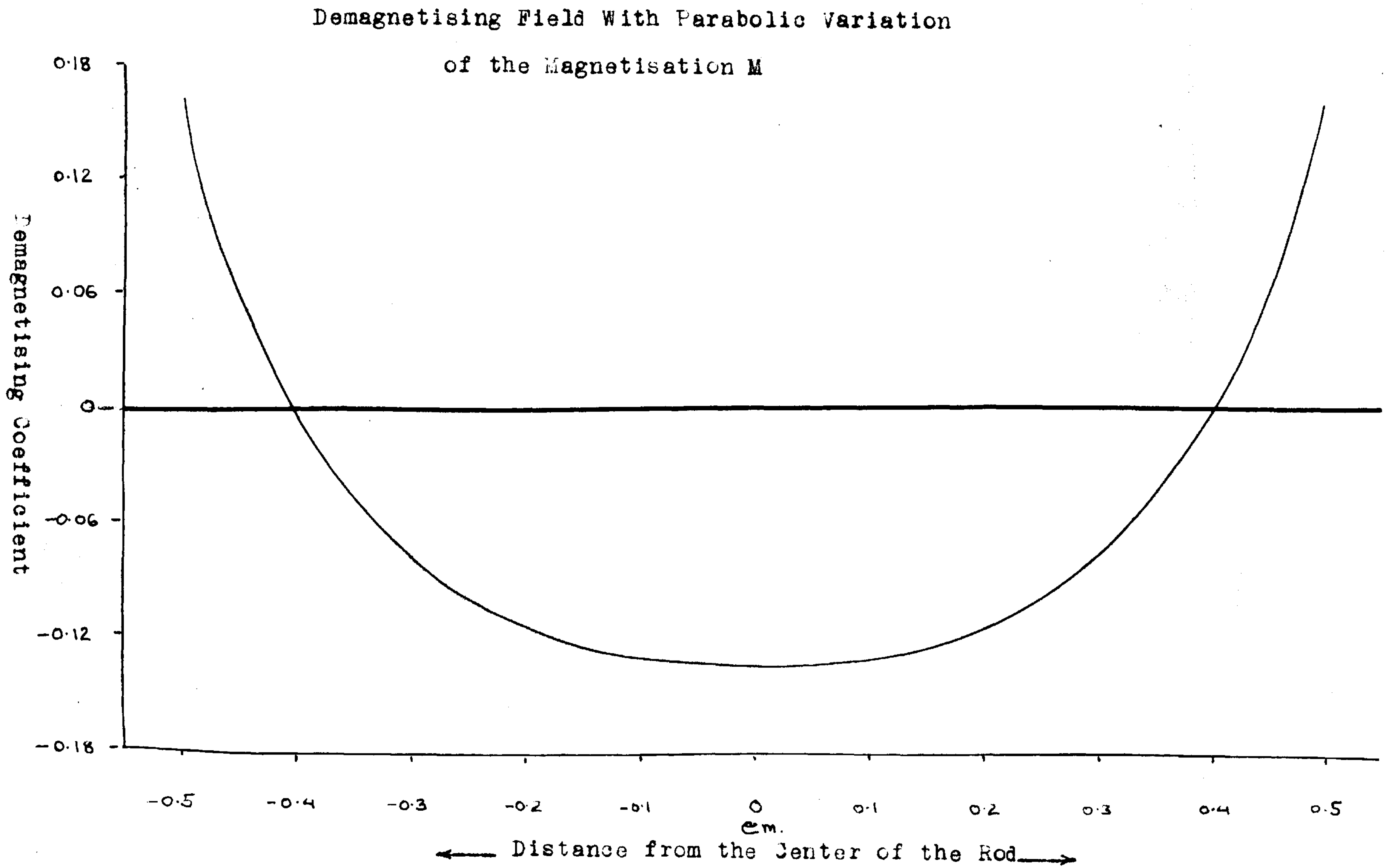
Demagnetising Field With Parabolic Variation
of the Magnetisation M
Demagnetising Coefficient
0·18
0·12
0·06
0
-0·06
-0·12
-0·18
-0·5
-0·4
-0·3
-0·2
-0·1
0
0·1
0·2
0·3
0·4
0·5
cm.
Distance from the Center of the Rod

FIGURE (5-7)

Considering a typical frequency, say 970 Mc/s, the delayed pulse begins to appear at $H_{ext.} = 485$ Oersteds and -

$$\frac{\omega}{\gamma} = 346 \text{ Oersteds}$$

$$H_a = \frac{2k_1}{M_s} \quad \text{for (100) direction}$$

Where $k_1$ is the anisotropy[19] constant, equal to $-6 \times 10^3$ erg/cm$^3$ for YIG at room temperature and $M_s$ is the saturation magnetisation ( $\simeq$ 140 Oersteds at room temperature).

$$H_a = -86 \text{ Oersteds}$$

$$Hi = 485 - 86 + H_d$$

$$= \frac{\omega}{|\gamma|} = 346$$

$$H_d \simeq -53 \text{ Oersteds}$$

For a resultant internal magnetic field to be in the neighbourhood of the above value at the ends,

$$M_n = 530 \text{ Oersteds}$$

$$M_1 = 1220 \text{ Oersteds}$$

These are obtained by making use of equations (5-9) and (5-13) and their computed curves. Having determined $M_n$ and $M_1$, the resultant demagnetising field is plotted by the equation:

$$H_d = H_{d1} + H_{d2}$$

Demagnetising Field With The Proposed Variation Of The

Magnetisation Vector

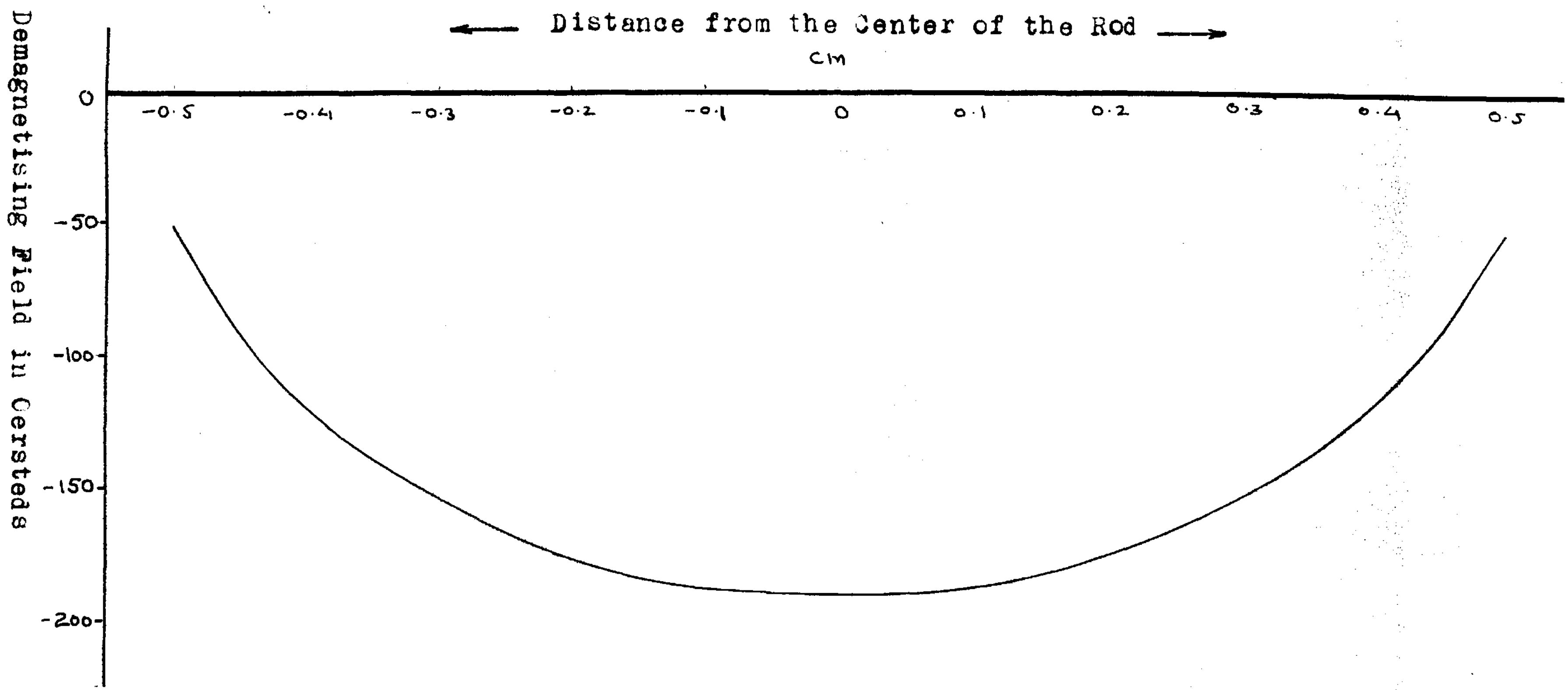


FIGURE (5-8)

$$H_d = H_{d1} + H_{d2} = 530 \left[ \frac{1-z}{\{(1-z)^2+a^2\}^{1/2}} + \frac{1+z}{\{(1+z)^2+a^2\}^{1/2}} - 2 \right]$$

$$1220/21 \left[ \{(z-1)^2+a^2\}^{1/2} + \{(z+1)^2+a^2\}^{1/2} + z^2 - 1^2/1 \right]$$

$$1220 \times 0.5/21 \left[ 2a^2 \log a - (z+1)\sqrt{(z+1)^2+a^2} \right.$$

$$- (1-z)\sqrt{(1-z)^2+a^2} - a^2 \log\left\{(z+1) + \sqrt{(z+1)^2+a^2}\right\} \times$$

$$\left. \left\{(1-z) + \sqrt{(1-z)^2+a^2}\right\} \right] \qquad (5\text{-}14)$$

This result is plotted in figure (5-8) making use of the IBM 7040 computer, and hence the internal magnetic field Hi is plotted making use of the relation (5-2). As discussed earlier, $H_{ext.}$ and $\omega/|\gamma|$ are nearly linearly related and so the same curve for demagnetising field holds for all the frequencies covered in our work.

The time delay $\tau$ is obtained by integrating the velocity between the turning points $\omega/\gamma$ i.e.

$$\tau = \int \frac{dz}{V_g(z)}$$

Vg(z) is given by the equation (5-1)

$$Vg(z) = \frac{1.06}{10^6} \left\{ \omega - \gamma (H_{ext.} + H_a + H_{d(z)}) \right\}^{3/2}$$

Internal Distribution of Magnetic Field Inside the Sample with

Proposed Variation of Magnetisation

$H_{ext}$ = 485 Oersteds

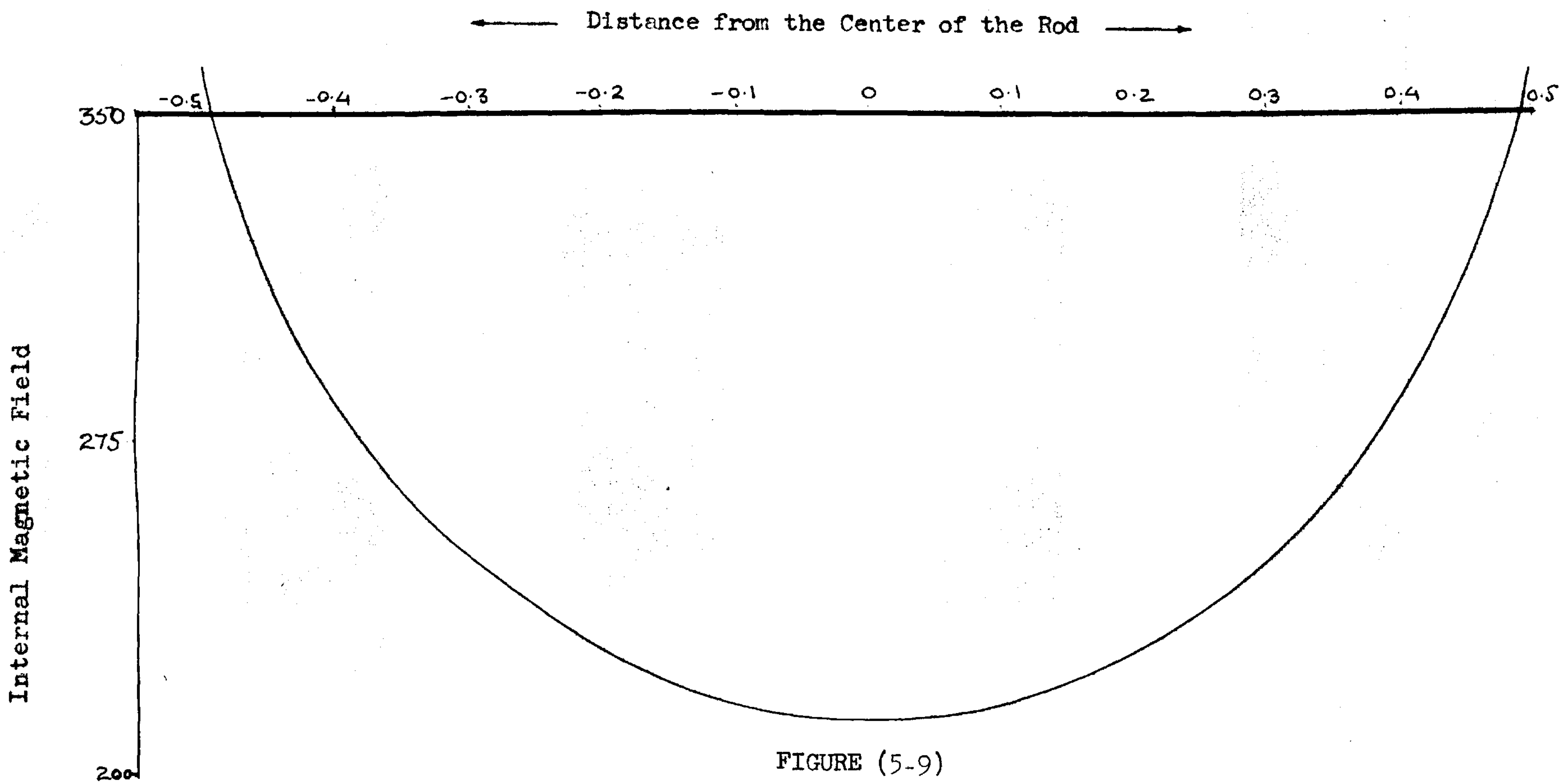


FIGURE (5-9)

It is extremely difficult to integrate this analytically in closed form. The delay time was computed by carrying out a numerical integration ( see computer prog. on p.75), making use of the IBM 7040 computer. The computed delay depends upon the interval dz chosen for a set of values for $M_n$ and $M_1$. This in turn gives a quantitative estimate of the region (in the vicinity of the turning point) in which the wave packet may be assumed to originate and then propogate to the other end.

For an interval dz = $10^{-6}$ cm. ( i.e. $k = 2\pi/\lambda = 2\pi \times 10^{6}$ $cm.^{-1}$ for $\lambda = 10^{-6}$ cm. -- which encompasses the limit for magnetostatic waves ) the computer calculation yields a delay of 1.7 $\mu$secs., at $M_n$ = 470 & $M_1$ = 1180 with a slope dH/dz = 700 Oe/cm. at the turning point ( appendix 1V ) . This delay decreases to 1.4 $\mu$secs for $M_n$ = 500 and $M_1$ = 1150 Oe. when the slope dH/dz increases to 825 Oe./cm. This results owing to a change of about 3 Oersteds in the external dc magnetic field. The constant component of magnetisation $M_n$ grows with increase in external field , making the slope of the curve for the internal magnetic field more gradual, and is accompanied by an increase in the delay.

# CHAPTER VI

## CONCLUSIONS

The low magnetic loss of single crystal Yttrium Iron Garnet allows wave propagation to take place at microwave frequencies within the crystal by means of magnetic waves, at room temperatures. A convenient method to excite such waves exists in the non uniformity of the demagnetising field of a non-ellipsoidal sample.

Experiments have been performed on a cylindrical YIG crystal sample 0.402 inch long, and 0.125 inch diameter. A strip line, two port-transmission type coupling assembly was designed and fabricated to excite magnetostatic waves in the sample. A suitable mount was also designed to hold the coupling assembly so that the YIG crystal could be oriented precisely in an external magnetic field.

Magnetostatic waves of frequency of 950 MHz were observed to propagate when the external magnetic field was in the neighbourhood of 500 Oersteds. The YIG sample was magnetised axially along the (100) direction and at room temperature. The time delay for these waves to propagate through the crystal varied from nearly zero to less than two microseconds for a field variation of 4 Oersteds.

As discussed in chapter 5, section 5.2 these waves require a concave shape for the internal magnetic field in order to propagate in the transmission type device used. Also the value of the applied dc magnetic field at which the magnetostatic waves were observed, (i.e. 500 Oersteds) is much below the saturation value of 1750 Oersteds for YIG at room temperature.

A non-uniform distribution of magnetisation is therefore proposed for the unsaturated sample to explain the excitation, propagation and delay of the magnetostatic waves at the observed frequencies and the applied dc magnetic fields. It is assumed that the magnetisation has two components in the direction of the applied field, one which is uniform along the length of the sample and the other varying parabolically. This extends the hitherto simplified relation used by Strauss etc. which relates the potential function with magnetisation, viz.,

$$\psi = -\int \frac{\operatorname{div} M}{r}\, d\tau - \int \frac{M_n}{r}\, d\sigma$$

as described in chapter 5, section 5.3.
For uniform magnetisation, div M = 0 and only $M_n$ contributes to the potential. However, in the proposed magnetisation, both the terms contribute to the potential function.

In qualitative terms this variation is feasible if we assume that the rf magnetic field at the ends makes the distribution of domains more in a random fashion compared with those at the center of the specimen so that the net magnetisation tends to be higher in the center. This model gives a field distribution with a value of $\omega/\gamma$ at ends and concave shape within the sample to enable wave propagation to take place.
It also infers that the internal magnetic field and therefore the wave propagation would be a function of the applied rf field and this aspect is worthy of further experimental work.

The time delay for waves in this proposed field was computed by carrying out numerical integration using an IBM 7040 Computer, and agrees with the experimental results. This computation has shown that most of the delay is confined to the end regions where $\omega/\gamma = H$ is very nearly equal to the internal magnetic field: about 98% of delay occurs over 2% of the rod length. This indicates that the delay characteristics of the magnetostatic waves will be practically independent of the rod length, assuming a similar internal field distribution.

As discussed in chapter 2 the time delay of propagating waves depends on the value of their wave vector k which lies within the range:

$k < 10$ for electromagnetic wave propagation.

$10 < k < 10^5$ for magnetostatic waves.

$k > 10^5$ for exchange dominated spin waves.

To obtain long time delays with magnetostatic waves, it is advantageous to provide a more gradual slope for the demagnetising field. As most of the delay is confined near the ends of the crystal, modification of the crystal structure near the end surfaces may provide a means to achieve this. Alternatively, for long time delays, spin wave propagation should be utilized or the propagation characteristics of lower frequencies be investigated. However, for spin wave propagation, the coupling mechanism has to be very efficient as electromagnetic energy with wavelength in the cm. range has to be converted to spin wavelengths which are in the micron range. Moreover, crystal imperfections and dislocations have to be much smaller compared to the spin wavelengths involved to keep the scattering to a minimum. In our experimental set up, only magnetostatic waves were observed. To observe spin waves, a more efficient coupling system with a possible provision for the rotation of the crystal with respect to the coupling loops is desirable.

# APPENDIX I

The macroscopic equation of motion for spinning electrons is

$$\frac{d\vec{M}}{dt} = \gamma \left( \vec{M} \wedge \vec{H}_{eff} \right) \qquad \text{where}$$

$M$ = magnetisation vector at a point ( magnetic moment per unit volume ) and is equal to

$M = M_o + m$

$H_{eff}$ = vector sum of all the magnetic fields seen by the spinning electrons and is equal to

$H = H_o + h$

$m_1$, $h$, $e$, arise because of the rf magnetic field ( applied perpendicular to the sample )

$$h = \vec{h} \text{ exp. } i \left( wt + \vec{k}.r \right)$$

$$e = \vec{e} \text{ exp. } i \left( wt + \vec{k}.r \right)$$

$$m_1 = \vec{m}_1 \text{ exp. } i \left( wt + \vec{k}.r \right)$$

The exchange energy density is taken as $1/2 \; B \left| \nabla M (r) \right|^2$ Anisotropy energy for the time being is ignored. The internal dc magnetic field is along the $z$ - direction, assumed to be uniform . Neglecting any loss term , the equation of motion has the form

$$i \times \frac{wm}{\gamma} = M_o \wedge \left( h - B \; \vec{k}.\vec{k} \; m \right) - H_i \wedge m$$

From the Maxwell's equations

$$\text{curl}\ \vec{E} = -1/c\ \ \partial\vec{B}/\partial t$$

$$\text{curl}\ \vec{H} = \vec{J} + \frac{\partial\vec{D}}{\partial t}$$

we have

$$\text{curl}\ \left[ e\ \exp.\ i\ (\ wt + \vec{k}.\vec{r}\ ) \right] = -\frac{w}{c}\ (\ h + 4\pi m\ )\ i\ \exp.\ i\ (\ wt + \vec{k}.\vec{r}\ )$$

$$\nabla \wedge (\ A\ \phi\ ) = \phi\ (\nabla \wedge A\ ) + (\nabla \phi\ ) \wedge A$$

therefore, $\text{L. H. S.} = \exp\ i\ (wt + \vec{k}.\vec{r}.)\ [\nabla \wedge e] + \nabla \{\ \exp.\ i\,(wt + \vec{k}.\vec{r})\} \wedge e$

$$= 0 + [\exp.\ i\ (\ wt + \vec{k}.\vec{r}\ )]\ \vec{k} \wedge \vec{e}$$

$$= \vec{k} \wedge \vec{e}$$

similarily

$$\vec{k} \wedge h = \frac{w}{c}\ \epsilon\ e$$

eliminating $e$ we have

$$(\ \vec{k}.h\ )\ \vec{k} - (\vec{k}.\vec{k}\ )\ h = -\frac{w^2}{c^2}\ \epsilon\ (\ h + 4\pi m\ ) \qquad (\text{A-1})$$

The equations of motion have solutions

$$\left[ \pm \frac{w}{\gamma} + H_i + M_o B\ (\ \vec{k}.\vec{k}) \right] m^{\pm} = M_o\ h^{\pm} \qquad (\text{A-2})$$

$$m^z = 0$$

The characteristic equation is now found by eliminating $h$ $m$ between (A-1) and (A-2) which is

$$\frac{1}{k_x^2 + k_y^2} + \frac{1}{2} \left[ \frac{(\vec{k}.\vec{k} - k_o^2\ )}{4\pi M_o} \left( \frac{w}{\gamma} + H_i + M_o B\ (\ \vec{k}.\vec{k}) \right) - k_o^2 \right]^{-1}$$

$$+ \frac{1}{2} \left[ \frac{(\vec{k}.\vec{k} - k_o^2\ )}{4\pi M} \left( -\frac{w}{\gamma} + H_i + M_o B\ (\vec{k}.\vec{k}) - k_o^2 \right) \right]^{-1} = 0 \qquad (\text{A-3})$$

where $k_o^2 = (\ w^2 / c^2\ )\ \epsilon$

In the absence of propogation effects , $k = 0$ and it follows from (A-3)

$$(w/\gamma)^2 = (H_i + M_0 B\ \vec{k}.\vec{k})\left[(H_i + M_0 B\ \vec{k}.\vec{k} + 4\pi M\left(\frac{k_x^2 + k_y^2}{k.k}\right)\right]$$

This may be written in the form

$$(w/\gamma)^2 = (H + Dk^2)\ (H + D\,k^2 + 4\pi M\,(k_x^2 + k_y^2)/\,k^2$$

$$k^2 = k_x^2 + k_y^2 + k_z^2$$

$D = M_0 B$ = a phenomenological constant , M being the saturat ion magnetisation and B (positive in ferro- ferrimagnetic medium) and B is a phenomenological quantity .

## APPENDIX II

Neglecting electromagnetic propogation ,

$$\text{curl } h = 0$$

This implies a scalar magnetic potential $\Psi$ , where

$$h = \nabla \Psi$$

Also div b = div ( h + 4 π m ) = 0

$$\nabla^2 \Psi + 4\pi \nabla \cdot m = 0$$

Therefore, $(1 + K)\left[\frac{\partial^2 \Psi}{\partial x^2} + \frac{\partial^2 \Psi}{\partial y^2}\right] + \frac{\partial^2 \Psi}{\partial z^2} = 0$ inside the sample

$$\frac{\partial^2 \Psi}{\partial x^2} + \frac{\partial^2 \Psi}{\partial y^2} + \frac{\partial^2 \Psi}{\partial z^2} = 0 \qquad \text{outside the sample}$$

Following Fletcher and Kittel's approach , this scalar potential function $\Psi$ has solutions in cylindrical coordinates as

$$\Psi_{in} = A_{in} \, J_n\left[\frac{i k \rho}{(1 + K)^{1/2}}\right] \exp.(i k z) \exp.(i n \phi)$$

$$\Psi_{out} \propto H_n^{(1)}(ik\rho) \exp.(ikz) \exp(in\phi)$$

where $H_n^{(1)}$ is a Hankel function; here

$$K = \frac{4 \pi M_0 H_0}{H_0^2 - (w/\gamma)^2}$$

In the short-wavelength limit $k\rho \gg 1$ we may approximate the Hankel function by

$$H_n^{(1)}(ik\rho) \propto (k\rho)^{-1/2} \cdot \exp.(-k\rho)$$

so that

$$\Psi_{out} \cong A_{out} (k\rho)^{-1/2} \cdot \exp.(-k\rho) \exp.(in\phi) \exp.(ikz)$$

The boundar y condition on the continuity of the tangential component of H at the surface $\rho = R$ is satisfied provided

$$A_{in}\, J_n\left[\frac{ikR}{(1+K)^{1/2}}\right] = A_{out}\,(kR)^{-1/2} \times \exp.(-kR) \qquad (1)$$

The boundary condition on the normal componentof B is

$$(1+K)\left(\frac{\partial\psi_{in}}{\partial\rho}\right) - (i\nu/R)\,(\partial\psi_{in}/\partial\phi) = \partial\psi_{out}/\partial\rho \qquad (2)$$

where

$$\nu = \frac{4\pi M\ (w/\gamma)}{H - (w/\gamma)}$$

From (2) we have , for $kR \gg 1$,

$$A_{in}\Big\{(1+K)\left[ik/(1+K)^{1/2}\right] J_n'\left[ikR/(1+K)^{1/2}\right]$$
$$+(n\nu/R)\, J_n\left[ikR/(1+K)^{1/2}\right]\Big\} = -A_{out}\,(k/R)^{1/2}\exp.(-kR) \quad (3)$$

Combining (1) and (3) ,

$$i\,(1+K)^{1/2}\,(J_n'/J_n) = -1 - (n\nu/kR) \qquad (4)$$

This is the characteristic equation , where the argument of the Bessel function is $ikR/(1+K)^{1/2}$ .

For excitation by an interaction which is uniform across the specimen we may set $n=1$. We set

$$\frac{(w-\gamma H_o)}{4\pi\gamma M_o} = \epsilon$$

For $kR \gg 1$ , it is seen that $\epsilon \ll 1$; then

$$K \cong \nu \cong -1/2\,\epsilon$$

and (4) becomes , for $n=1$, with $x = (2\epsilon)^{1/2}\,kR$,

$$J_1'(x)\,/\,J_1(x) = -1/x,$$

which may be reduced to

$$J_o(x) = 0$$

The three lowest roots are $x = 2.405$ ; $5.520$ ; and $8.654$ ; the lowest corresponding eigenfrequency is

$$w = \gamma H + 2\pi\gamma M\,(2.405/kR)^2$$

# APPENDIX III

$$4\pi\Psi = \frac{M_1}{\ell^2}\iiint \frac{\varepsilon_e}{r}\, d\varepsilon_e\, d\sigma$$

$$= \frac{M_1}{\ell^2}\int_{-\ell}^{\ell} \varepsilon\, d\varepsilon_e \int_0^a \frac{\rho\, d\rho}{\{(z-\varepsilon_e)^2+\rho^2\}^{1/2}} \int_0^{2\pi} d\varphi$$

Or $$\Psi = \frac{M_1}{2\ell^2}\int_{-\ell}^{\ell} \varepsilon_e\, d\varepsilon_e \left[\left\{(z-\varepsilon_e)^2+a^2\right\}^{1/2} - |z-\varepsilon_e|\right]$$

$$= \text{First term} - \frac{M_1}{2\ell^2}\left[\int_{-\ell}^{z}(z-\varepsilon_e)\,\varepsilon_e\, d\varepsilon_e + \int_{z}^{\ell}(\varepsilon_e - z)\,\varepsilon_e\, d\varepsilon_e\right]$$

$$= F.T + \frac{M}{2l}\left(\frac{1}{3}z^3 - z\,l^2\right)$$

$$H_{d_z} = -\frac{\partial\psi}{\partial z} = \frac{M_1}{2\ell^2}\int_{-\ell}^{\ell}\varepsilon_e\, d\varepsilon_e\,\frac{\partial}{\partial\varepsilon_e}\left[(z-\varepsilon_e)^2+a^2\right]^{1/2} + \frac{M_1}{2\ell^2}(z^2-\ell^2)$$

**The second term of equation (5-12) is**

$$-\frac{M_1}{2\ell^2}\int_{-\ell}^{z}\sqrt{(z-\varepsilon_e)^2+a^2}\; d\varepsilon_e - \frac{M_1}{2\ell^2}\int_{z}^{\ell}\sqrt{(\varepsilon_e-z)^2+a^2}\; d\varepsilon_e$$

Now $$\int\sqrt{x^2+a^2}\,dx = \frac{1}{2}\left[x\sqrt{x^2+a^2} + a^2\log\left(x+\sqrt{x^2+a^2}\right)\right]$$

Let $z-\varepsilon_e = x$ , $d\varepsilon_e = dx$

$\varepsilon_e - z = y$ , $d\varepsilon_e = dy$

Hence the above integral yields

$$\frac{M_1}{2\ell^2}\left[(z-\varepsilon_e)\sqrt{(z-\varepsilon_e)^2+a^2} + a^2\log\left[(z-\varepsilon_e)+\sqrt{(z-\varepsilon_e)^2+a^2}\right]\right]_{-\ell}^{z} -$$

$$\frac{M_1}{2\ell^2}\left[(\varepsilon_e-z)\sqrt{(\varepsilon_e-z)^2+a^2} + a^2\log\left[(\varepsilon_e-z)+\sqrt{(\varepsilon_e-z)^2+a^2}\right]\right]_{z}^{\ell}$$

= value given in text

# APPENDIX 1V

For the constant component $M_n$

$$H = 0.5M_n\left\{\frac{l-z}{\sqrt{(l-z)^2 + a^2}} + \frac{l+z}{\sqrt{(l+z)^2 + a^2}} - 2\right\}$$

$$\frac{dH}{dz} = 0.5\,M_n\left[\frac{(l-z)^2}{\{(l-z)^2+a^2\}^{3/2}} - \frac{1}{\{(l-z)^2+a^2\}^{1/2}} - \frac{(l+z)^2}{\{(l+z)^2+a^2\}^{3/2}} + \frac{1}{\{(l+z)^2+a^2\}^{1/2}}\right]$$

$= -\,3.14\,M_n$ for $l=z$, $a=0.15875$ cm., $l= 0.5105$ cm.

For the varying component $M_1$

$$H = 0.25\,M_1/l^2\left[2a^2\log a-(z+l)\sqrt{(z+l)^2 + a^2} - (l-z)\sqrt{(l-z)^2 + a^2} - a^2\log\left\{(z+l) + \sqrt{(z+l)^2 + a^2}\right\}\left\{\sqrt{(l-z)^2 + a^2} + (l-z)\right\}\right]$$

$$\frac{dH}{dz} = 0.5\,M/l^2\left[\frac{z(z-l) + a^2}{\{(z-l)^2 + a^2\}^{1/2}} - \frac{z(z+l) + a^2}{\{(z+l)^2 + a^2\}^{1/2}} + 2z\right]$$

$= 0.65\,M_1$ for $z=l$ and values of $a$ and $l$ as used above.

Hence the slope $dH/dz$ of the internal magnetic field with the proposed variation of magnetisation is

$$\frac{dH}{dz} = 0.65M_1 - 3.14\,M_n$$

$= -\,700$ Oe/cm. for $M_n = 470$ and $M_1 = 1180$

$= -\,825$ Oe/cm. for $M_n = 500$ and $M_1 = 1150$

```
$JOB            003503 CM KUDSIA            C60
$IBJOB          NODECK
$IBFTC
C       DEMAGNETISING FIELDS WITH UNIFORM MAGNETISATION (CONSTANT--M) AND
C       WITH PARABOLIC VARIATION OF MAGNETISATION (M=C(1-Z*Z/L*L))
        REAL L
        A=0.15875
        L=0.5105
        AA=A*A
        PRINT 4
      4 FORMAT(10X,20HDISTANCE FROM CENTRE, 10X,22HDEMAG COEFF-CONSTANT M,
       110X,23HDEMAG COEFF-PARABOLIC M///)
        Z=0.0
      2 Z1=Z-L
        Z2=Z1*Z1+AA
        Z2R=SQRT(Z2)
        ZA=Z+L
        ZB=ZA*ZA+AA
        ZBR=SQRT(ZB)
        ZZ=Z2R+ZBR+(Z*Z-L*L)/0.5105
        C1=(Z+L)*ZBR
        C2=(L-Z)*Z2R
        C3=Z+L+ZBR
        C3L=ALOG(C3)
        C4=L-Z+Z2R
        C4L=ALOG(C4)
        CC=(2.0*AA)*ALOG(A)-C1-C2-AA*C3L-AA*C4L
        HS=0.5*100.0*((L-Z)/Z2R+(L+Z)/ZBR-2.0)
        HR=100.0*(ZZ/L+CC/(2.0*L*L))
        PRINT 1, Z, HS, HR
      1 FORMAT(15X, F10.5, 22X,F10.5, 25X,F10.5/)
        Z=Z+0.025
        IF(Z.GT. 0.5) GO TO 3
        GO TO 2
      3 STOP
        END
$ENTRY
$IBSYS

                                CD TOT    0038
```

```
$JOB    WATFOR   003503 CK KUDSIA              060
$IBJOB          NODECK
$IBFTC
C       MICROWAVE TIME DELAY BY NUM. INTEG. WITH PROPOSED VARIATION OF M
        REAL L
        F=2.0*3.1416*970.E06
        G=1.76E07
        T1=0.637E-07
        A=0.15875
        L=0.5105
        AA=A*A
        FF=(2.0*AA)*ALOG(A)
        PRINT 4
      4 FORMAT(10X,20HDISTANCE FROM CENTRE,10X,19HDEMAGNETISING FIELD,
       110X,14HINTERNAL FIELD,10X,8HVELOCITY,10X,10HTIME DELAY/////)
        Z=0.49616
      2 Z1=L-Z
        Z2=Z1*Z1+AA
        Z2R=SQRT(Z2)
        ZA=Z+L
        ZB=ZA*ZA+AA
        ZBR=SQRT(ZB)
        ZZ=Z2R+ZBR-(Z1*ZA)/0.5105
        C1=ZA*ZBR
        C2=Z1*Z2R
        C3=ZA+ZBR
        C3L=ALOG(C3)
        C4=Z1+Z2R
        C4L=ALOG(C4)
        CC=FF-C1-C2-AA*C3L-AA*C4L
        HR=1165.0*(ZZ/L+CC/0.5212205)
        HS=243.0*(Z1/Z2R+ZA/ZBR-2.0)
        HD=HS+HR
        HI=392.0+HD
        F1=ABS(F-G*HI)
        V=1.06*(F1**1.5)/1.0E06
        T1=0.000001/V+T1
        Z=Z+0.000001
        IF (Z. GT. 0.49632) GO TO 3
      1 PRINT 8, Z, HD, HI, V, T1
      8 FORMAT(15X,F10.6, 20X,F10.6,16X,F10.6,12X,E12.6,7 X,E10.6)
        GO TO 2
      3 STOP
        END
$ENTRY
$IBSYS

                                   CD TOT    0046
```

BIBLIOGRAPHY

1. Pomerantz, M. "Ultrasonic Loss and Gain Mechanisms in Semiconductors" Proc. I.E.E.E., Vol 53, No. 10, pp. 1438, October 1965.

2. Rollins, F.R. "Phonon Interactions at Ultrasonic Frequencies" Proc. I.E.E.E., Vol. 53, No. 10, pp. 1534, October 1965.

3. Quate, C.F. ET.AL. "Interaction of Light and Microwave Sound" Proc. I.E.E.E., Vol. 53, No. 10, pp. 1604, October 1965.

4. Bolef, D.I. and Sundfors, R.K. "Interaction of Acoustic Waves with Nuclear Spins in Solids" Proc. I.E.E.E., Vol. 53, No. 10, pp. 1574, October 1965.

5. Tehon, S.W. and Wanuga, S. "Microwave Acoustics" Proc. I.E.E.E., Vol. 52, No. 10, October 1964.

6. Akhiezer, A.I. "Kilomegacycle Ultrasonics" by Klaus Dransfeld, Scientific American , vol. 208, No.6 PP 60- 68, June 1963

7. Lax and Button "Microwave Ferrites and Ferri-magnetics" McGraw-Hill Book Company, Inc. 1962 P 125

8. Nielson, J.W. and Dearborn, E.F. "The Growth of Single Crystals of Magnetic Garnets" J. Phys. Chem. Solids, Vol. 5, pp. 202 - 207, 1958.

9. Baranskii, K.N. Soviet Phys. Doklady, Vol. 2, pp. 237, July 1958.

10. Bommel, H.E. and Dransfeld, K. "Excitation of Hypersonic Waves by Ferromagnetic Resonance" Phys. Rev. Lett., Vol. 3, No. 2, pp. 83, 1959.

11. Foster, N.F. "Cadmium Sulphide Evaporated-Layer Transducers" Proc. I.E.E.E., Vol. 53, No. 10, pp. 1400, October 1965.

12. Foster, N.F. "Ultra-High Frequency Cadmium Sulphide Transducers" I.E.E.E. Transactions on Sonics and Ultrasonics, Vol. SU-11, No. 2, November 1964

13. Seavey, Jr. M.H. "Microwave Phonon Generation by Thin Magnetic Films" Research Report, February 1963, U.S. Air Force, L.G. Hanscom Field. Mass.

14. Walker, L.R. "Spin Waves and Other Magnetic Modes" Magnetism, Vol, 1, G.T. Rodo and H. Suhl, Eds. New York , Academic, 1963, pp. 299 - 381.

15. Schlömann, E. "Generation of Spin Waves in Non-Uniform Magnetic Fields I. Conversion of Electromagnetic Power into Spin Wave Power and Vice Versa" J. Appl. Phys., Vol. 35, No. 1, pp. 159 - 166, January 1964.

16. Sommerfeld, A. "Electrodynamics" pp. 82, Academic Press Inc., New York, N.Y., 1952.

17. Fletcher, P.C. and Kittel, C. "Considerations on the Propagation and Generation of Magnetostatic Waves" Phys. Rev., Vol. 120, No. 6, pp. 2004, December 1960

18. Lax, B. and Button, K.J. "Microwave Ferrites and Ferrimagnetics" McGraw - Hill Book Company, Inc., 1962, pp. 320.

19. Morrish, A.H. "The Physical Principles of Magnetism" pp--520 ,John Wiley and Sons,Inc., New York ,N.Y.,1965

20. Oberhettinger, F. and Magnus, W. "Anwendung der Elliptishen Functioner in Physik und Technik" Springer, 1949

21. John, S.B. "Problems in Strip transmission lines" Special Issue on Microwave Theory and Techniques, March 1955, pp. 124.

22. Strauss, W. "Magnetoelastic Waves in Yttrium Iron Garnet" J. Appl. Phys., Vol. 36, No. 1, pp. 118 - 123, January 1965.